Bull Volcanol (2007) 70:1–22
DOI 10.1007/s00445-007-0120-y

REVIEW PAPER

Lava effusion rate definition and measurement: a review

Andrew J. L. Harris · Jonathan Dehn · Sonia Calvari

Received: 15 December 2005 / Accepted: 3 January 2007 / Published online: 10 March 2007

Abstract Measurement of effusion rate is a primary objective for studies that model lava flow and magma system dynamics, as well as for monitoring efforts during on-going eruptions. However, its exact definition remains a source of confusion, and problems occur when comparing volume flux values that are averaged over different time periods or spatial scales, or measured using different approaches. Thus our aims are to: (1) define effusion rate terminology; and (2) assess the various measurement methods and their results. We first distinguish between instantaneous effusion rate, and time-averaged discharge rate. Eruption rate is next defined as the total volume of lava emplaced since the beginning of the eruption divided by the time since the eruption began. The ultimate extension of this is mean output rate, this being the final volume of erupted lava divided by total eruption duration. Whether these values are total values, i.e. the flux feeding all flow units across the entire flow field, or local, i.e. the flux feeding a single active unit within a flow field across which many units are active, also needs to be specified. No approach is without its problems, and all can have large error (up to ~50%). However, good agreement between diverse approaches shows that reliable estimates can be made if each approach is applied carefully and takes into account the caveats we detail here. There are three important factors to consider and state when measuring, giving or using an effusion rate. First, the time-period over which the value was averaged; second, whether the measurement applies to the entire active flow field, or a single lava flow within that field; and third, the measurement technique and its accompanying assumptions.

Keywords Lava · Instantaneous effusion rate · Time-averaged discharge rate · Eruption rate · Monitoring

Editorial responsibility: C Kilburn

A. J. L. Harris (✉)
HIGP/SOEST, University of Hawai'i,
1680 East West Road,
Honolulu, HI 96822, USA
e-mail: harris@higp.hawaii.edu

J. Dehn
Alaska Volcano Observatory, Geophysical Institute,
University of Alaska Fairbanks,
Fairbanks, AK 99775, USA

S. Calvari
Instituto Nazionale di Geofisica e Vulcanologia,
Sezione di CataniaPiazza Roma 2,
95123 Catania, Italy

Introduction

The rate at which lava is erupted is commonly termed effusion rate. Upon eruption, lava may not necessarily flow across the surface, but can be tube-contained and/or injected into the interior of a flow or dome to cause inflation or endogenous growth (Calvari and Pinkerton 1998, 1999; Fink 1993; Fink et al. 1990; Fink and Griffiths 1998; Glaze et al. 2005; Greeley 1987; Guest et al. 1984; Hon et al. 1994; Iverson 1990; Kauahikaua et al. 1998; Mattsson and Höskuldsson 2005; Nakada et al. 1995; Ollier 1964; Peterson et al. 1994; Rossi and Gudmundsson 1996; Self et al. 1996, 1997; Thordason and Self 1996, 1998; Walker 1991). Whether exogenously or endogenously emplaced, effusion rate controls the way in which a lava body grows, extends and expands, influencing its dimensional properties, such as length, width, thickness, volume and/or area (Baloga and Pieri 1986; Blake 1990; Blake and Bruno 2000; Fink and Bridges 1995; Kilburn 2000; Kilburn

and Lopes 1988; Kilburn et al. 1995; Malin 1980; Mayamoto and Sasaki 1998; Murray and Stevens 2000; Pieri and Baloga 1986; Pinkerton and Wilson 1994; Stasiuk and Jaupart 1997; Swanson and Holcomb 1990; Wadge 1978; Walker 1973). Effusion rate also influences pressure conditions within an inflating unit and the morphology of the flow surface (Anderson et al. 1998; Denlinger 1990; Fink and Griffiths 1992, 1998; Gregg and Fink 2000; Griffiths and Fink 1992; Iverson 1990; Rowland and Walker 1990). In addition, effusion rate and flow velocity affects flow heat loss and cooling, and hence crystallization rates (Crisp and Baloga 1994; Dragoni 1989; Dragoni and Tallarico 1994; Dragoni et al. 1992; Harris et al. 1998, 2005; Keszthelyi 1995; Keszthelyi and Self 1998; Pieri and Baloga 1986; Sakimoto and Zuber 1998). Thus, effusion rate, velocity and volume are important input parameters into lava flow models and simulations, and/or have been the outputs of others (e.g. Costa and Macedonio 2005; Crisci et al. 2003, 2004; Favalli et al. 2005; Glaze and Baloga 2001; Harris and Rowland 2001; Hikada et al. 2005; Ishihara et al. 1990; Keszthelyi and Self 1998; Keszthelyi et al. 2000; Macedonio and Longo 1999; Rowland et al. 2004, 2005; Wadge et al. 1994; Young and Wadge 1990). Finally, by representing material supplied from a deeper source, effusion rates allow constraint of mass flux out of the shallow feeder system, allowing assessment and/or modelling of the mass balance and dynamics of the effusing or extruding system, and of the source depth and conduit geometry (e.g. Allard 1997; Allard et al. 1994; Barmin et al. 2002; Denlinger 1997; Denlinger and Hoblitt 1999; Dvorak and Dzurisin 1993; Dzurisin et al. 1984; Francis et al. 1993; Harris and Stevenson 1997; Harris et al. 2000, 2003; Melnik and Sparks 1999, 2005; Naumann and Geist 2000; Ripepe et al. 2005; Rowland and Munro 1993; Rowland et al. 2003; Wadge 1977, 1981–1983; Wadge et al. 1975).

All of these factors make measurement of effusion rate a primary objective not just for studies that aim to understand and model lava flows and shallow system dynamics, but also for monitoring efforts during on-going eruptions (e.g. Barberi et al. 1993; Andronico et al. 2005; Calvari and INGV-Catania 2001; Calvari et al. 1994, 2003, 2005; Kauahikaua et al. 2003; Sutton et al. 2003). Effusion rates can be used, for example, to determine whether activity is waxing or waning (Harris et al. 2000; Wadge 1981) or to assess the long-term behaviour, and eruptive/hazard potential, of a system (Branca and Del Carlo 2005; Wadge 1977, 1981, 1983; Wadge et al. 1975). They can also be used in predictive models designed to estimate the possible extent, and thus hazard posed by, advancing flows (e.g. Calvari and Pinkerton 1998; Costa and Macedonio 2005; Crisci et al. 2003, 2004; Favalli et al. 2005; Ishihara et al. 1990; Rowland et al. 2005).

In spite of the importance of effusion rate, its definition can be a source of confusion, and problems occur when comparing volume fluxes averaged over different time periods, or measured using different approaches. This was the crux of the Tanguy et al. (1996) argument, which noted that variations in effusion rates measured during Etna's 1991–1993 eruption varied by a factor of 30. Some of the variation likely resulted from actual changes in the erupted flux; others, however, resulted from definition and measurement problems. The aims of this paper are to review and define a standard for effusion rate terminology, to collate and describe the various methods available for measuring effusion rates, and to discuss the value of timely effusion rate measurement in lava flow monitoring and hazard mitigation.

Definitions

Walker (1973) defined effusion rate as the instantaneous lava flow output by a vent, and eruption rate as the average lava output during a whole eruption. Subsequently there have been several interpretations of effusion rate and eruption (or discharge) rate, these terms often being used interchangeably, with eruption rates being averaged over a variety of time-periods from seconds to minutes, hours, days, months and years (e.g. Behncke and Neri 2003; Calvari et al. 1994; Fink et al. 1990; Glaze 1984; Harris and Neri 2002; Madeira et al. 1996; Nakada and Fujii 1993; Richter et al. 1970; Rowland and Munro 1993; Sutton et al. 2003; Swanson et al. 1979; Tanguy et al. 1996; Tilling et al. 1987; Wadge 1983; Wolfe et al. 1988; Zebker et al. 1996). This led Lipman and Banks (1987) to clarify that they were using "effusion rate" for instantaneous values, "discharge rate" for values averaged over a day, "mean effusion rate" for effusion rate averaged over a specified period of time, and "eruption rate" for values averaged over the whole eruption. This definition helps immensely in that it clearly defines the time over which the value is averaged (Fig. 1a).

Instantaneous effusion rate and time averaged discharge rate

Following Lipman and Banks (1987), instantaneous effusion rate can be defined as the volume flux of erupted lava that is feeding flow at any particular point in time. Such measurements, if made repeatedly over a short period of time, are useful in defining short-lived surges in the lava flux developing over seconds to minutes (e.g. Bailey et al. 2006; Guest et al. 1987; Harris and Neri 2002; Harris et al. 2006; Madeira et al. 1996; Lipman and Banks 1987) or for identifying detailed temporal trends in the erupted volume

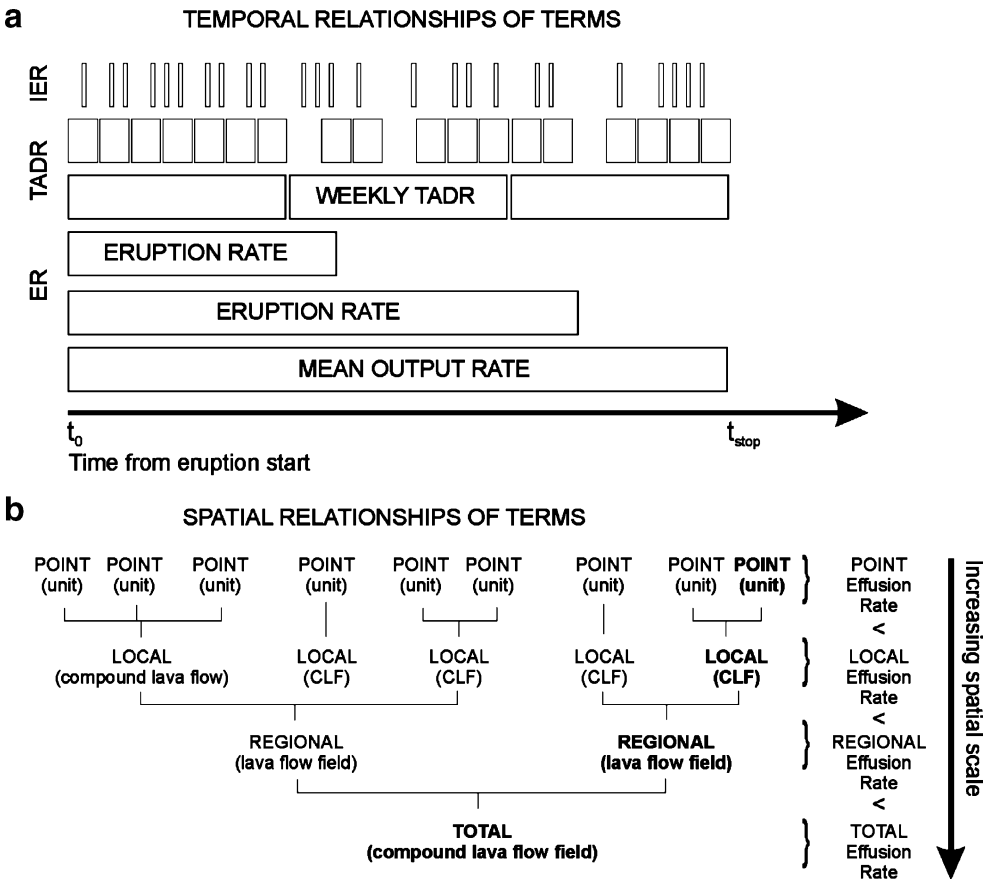

Fig. 1 Schematic showing **a** temporal, and **b** spatial scales to which each of our measurement definitions apply. *IER* = Instantaneous effusion rate, *TADR* = Time-averaged discharge rate, *ER* = eruption rate, t_0 = eruption start time, t_{stop} = eruption stop time, *CLF* = compound lava flow

flux developing over hours to days (e.g. Calvari et al. 2003, 2005; Frazzetta and Romano 1984; Harris et al. 2000; Wadge 1981).

We also distinguish between instantaneous volume flux measurements made at basaltic lava flows versus those made at silicic lava domes and flows, which we term instantaneous effusion rate for the former case and instantaneous extrusion rate for the later. This distinction stresses the viscosity, emplacement and morphological differences between the two cases. It is also consistent with the Chambers Dictionary definition of effusion, this being "pouring or streaming out; emission" versus that for extrude, i.e. "to force out, to expel; to protrude" so that extrusion is "the act of extruding, thrusting or throwing out" (Schwarz 1993). In both cases we have added the term "instantaneous" to avoid confusion over the temporal meaning of the phrase, underscoring the fact that the value is measured at a specific moment in time.

Time averaged discharge rates consider volume fluxes averaged over a given time period (Fig. 1a). This is typically obtained by measuring the volume emplaced over a known interval, and dividing by the duration to give volume flux over that interval (e.g. Andronico et al. 2005; Behncke and Neri 2003; Burton et al. 2005; Fink et al. 1990; Harris and Neri 2002; Jackson et al. 1975; Mazzarini et al. 2005; Nakada and Fujii 1993; Nakada et al. 1999; Richter et al. 1970; Rose 1972; Rossi 1997; Rowland 1996; Rowland et al. 1999; Sparks et al. 1998; Swanson and Holcomb 1990; Tilling et al. 1987; Wolfe et al. 1988; Zebker et al. 1996). For example, a daily discharge rate at a lava flow or dome may be obtained by dividing volume emplaced that day by 24 h (e.g. Behncke and Neri 2003; Zebker et al. 1996; Fig. 2a). Considering time-averaged values will begin to smooth any short-term variation in the instantaneous effusion rate. As we consider discharge rate averaged over longer time periods, the temporal detail diminishes (Fig. 2a). One advantage of this measurement over instantaneous effusion rate, however, is that short-term variations caused by short-lived changes in measurement conditions or bias introduced by the time of measurement can be minimized. For example, an instantaneous effusion rate measurement made during a short-lived surge in effusion is not representative of the typical flux for the longer time period (Bailey et al. 2006). As a result, time-averaged discharge rate allows identification of longer-term (month-to-decadal scale) trends and systematic changes (or similarities) in the system output (e.g. Behncke and Neri 2003; Burton et al. 2005; Fink et al. 1990; Nakada et al. 1999; Richter et al. 1970; Rose 1972; Swanson and Holcomb 1990; Wadge 1983; Wadge et al. 1975).

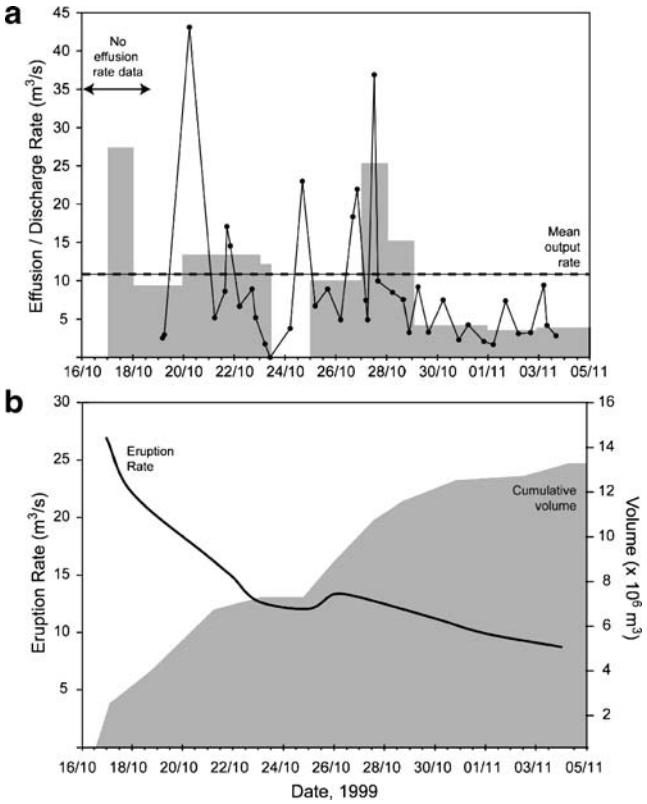

Fig. 2 **a** Instantaneous effusion rate (*black points and line*), time averaged discharge rate (*grey bars*) and mean output rate (*dashed*, *horizontal*, *line*) measured during the 17 October–5 November 1999 eruption from Etna's Bocca Nuova summit crater. The width of each discharge rate bar indicates the time period to which it applies. **b** Cumulative volume (*grey area*) and eruption rates (*black line*) derived for the same eruption. Data from Harris and Neri (2002)

Eruption rate and mean output rate

Eruption rate is defined here as the total volume of the lava emplaced since the beginning of the eruption divided by the time since the eruption began. The eruption rate on the 53rd day of an ongoing eruption, for example, is obtained by taking the volume emplaced up to day 53 divided by those 53 days (Fig. 1a). This differs from time averaged discharge rate in that time averaged discharge rates consider single flow units or volumes emplaced during discrete time windows within the eruption, whereas eruption rates considers all lava erupted since the start of the eruption.

The ultimate extension of the eruption rate is mean output rate (Barberi et al. 1993; Walker 1973). Mean output rate is the final volume of erupted lava divided by the total duration of the eruption (Fig. 1a). It can thus only be obtained when the eruption is over (e.g. Barberi et al. 1993; Guest et al. 1987; Jackson et al. 1975; Romano and Sturiale 1982; Rossi 1997; Rowland 1996; Swanson et al. 1979; Tanguy et al. 1996; Tilling et al. 1987). Mean output rate is the ultimate level of temporal smoothing and gives no detail regarding variations in effusion rate during the eruption (e.g. Fig. 2a).

Mean output rate is useful when comparing the volumetric flux of many eruptions, being a measure of the effusive intensity. Take, for example, the 1981 and 1984 eruptions of Mount Etna. These formed 12±3 and 19±4± 10^6 m^3 lava flow fields, respectively, (Harris et al. 2000). Thus, volumetrically, the 1984 event was more significant. If we consider, however, that these two eruptions lasted 7 and 172 days, respectively, we obtain mean output rates of 29 and 1.3 m^3/s. Thus, in terms of hazard, the 1981 event was more significant. Indeed, the 1981 flow advanced 8.8 km in just a few hours threatening the town of Randazzo (Guest et al. 1987; McClelland et al. 1989), whereas the 1984 flow remained confined to the summit, building a pile of short, overlapping flows no more than 3.3 km in length (Harris et al. 2000; McClelland et al. 1989).

Considerations

Short-term effusion rate variation

An important issue is whether a measurement made at a certain time is representative of that particular hour or day. In lava channels (and at flow fronts) flow velocity and depth can be highly variable over the time scale of minutes to hours (e.g. Bailey et al. 2006; Guest et al. 1987; Lipman and Banks 1987).

Short-term variations in observed flow depth/level or velocity (and hence derived effusion rate) may result from variations in supply, upstream blockage and blockage release, or changes in vesicularity (e.g. Bailey et al. 2006; Lipman and Banks 1987; Madeira et al. 1996). During the 1984 eruption of Mauna Loa, for example, Lipman and Banks (1987) noted that release of ponded volumes behind dams would cause down-flow velocities to suddenly increase from a few meters per minute to a few meters per second. During May 2001 we observed pulses in lava effusion at an Etnean lava channel due to variations in the bulk supply, as well as surges due to the failure of blockages (Bailey et al. 2006). Over a 2-day-long observation period, a series of 110–190-min-long cycles in effusion were observed, each involving a relatively long period of low effusion rate flow and terminating in a period of high effusion rate flow lasting 10–20 min. During the high effusion rate pulse, flow velocity was observed to increase by a factor of two over a time scale of 30 min (Fig. 3). Depth of the flow also increased, overflowing from the channel during a pulse to build a stack of pahoehoe overflow levées (Fig. 4a) and decreasing again so that the flow level was well below the levée rims between pulses (Fig. 4b). As a result, bulk effusion rate calculated from the flow width, depth and

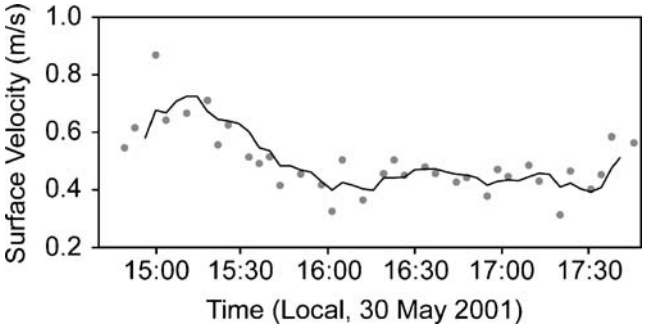

Fig. 3 Maximum surface flow velocity (with three-point-running-mean) as measured by Bailey et al. (2006) for the channel pictured in Fig. 4 for a 3.5-h-long period. Measurements were made by tracking pieces of crust in a series of thermal images

velocity varied from a low of 0.1 m^3/s between pulses to a peak of 0.9 m^3/s during pulses (Bailey et al. 2006).

Temporal and spatial considerations

Figure 1a summarizes the temporal nature of the terms, and the time scales over which each definition applies. The terms vary in how they use time. Instantaneous effusion rate, time-averaged discharge rate, eruption rate and mean output rate each consider volumes emplaced over increasing time periods as we move through the definition sequence. However, there are also spatial considerations because all of these measurements can be made on lava bodies at any spatial scale (Fig. 1b). Following the terminology of Walker (1973) a flow unit is the smallest spatial component of a lava flow field. It is a single, discrete body defined by margins that have cooled significantly and solidified before another flow-unit is superimposed upon it (Nichols 1936; Walker 1973). Such bodies include individual pahoehoe toes/lobes and single unit ′a′a flows. Compound lava flows and flow fields, however, are divisible into multiple flow units and multiple lava flows, respectively. Compound flows thus contain several zones of active units fed by a braided channel or tube system extending from a single vent as during the 1991 activity at Kalapana on Kilauea (Mattox et al. 1993). Likewise, a flow field will contain a number of compound flows. Where more than one active vent is present, a number of discrete zones of activity distributed around the volcano will form several compound flows at different locations as during the 2001 and 2002–2003 eruptions of Etna (Andronico et al. 2005; Behncke and Neri 2003; Calvari and INGV-Catania 2001). Together these form a total or compound lava flow field, which comprises every single flow unit erupted during the entire eruption. Thus, on the smallest spatial scale, a point or local effusion rate measurement will apply to a single flow unit within a compound lava flow, across which many units or flows may be active. On the largest spatial scale, the total volume

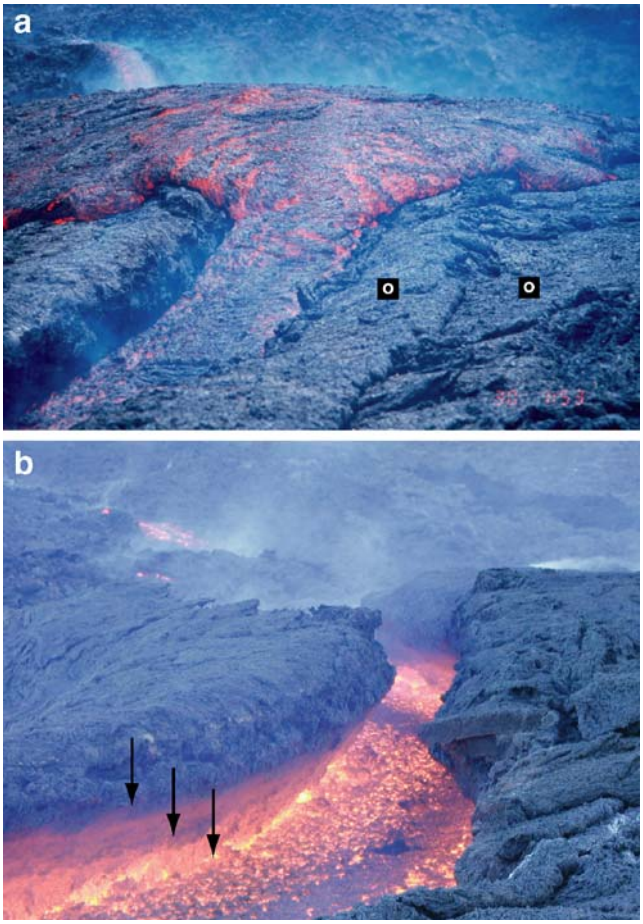

Fig. 4 **a** Pulse moving down a ~3 m wide channel on Etna during May 2001 (Bailey et al. 2006). A series of Pahoehoe overflow levées emplaced during previous pulses are apparent underlying the active pulse, and are marked "o." Pulse front is ~10 m wide. **b** The same channel during normal flow (Bailey et al. 2006). Note overhanging rims due to repeated overflow to construct a pile of overflow units that wrap around and over the channel rim. This causes the channel width to be narrowest at the levée rim (~1 m) and broaden downwards to an observable maximum of 3–4 m. *Black arrows* indicate high stand marks caused by lava accreted to the inner channel walls (at the flow surface–wall contact) during other higher (but below blank) flow levels

flux feeding all units across the entire compound flow field will give the total effusion rate for all active units (Fig. 1b).

Total effusion rate should thus be measured at the vent or at the master channel/tube before bifurcation if only one vent is active. If multiple sources are active, then the flux at each source must be measured and summed. At the smallest spatial scale, a local effusion rate applies to a single flow unit (Calvari et al. 1994). Local effusion rate thus represents the instantaneous volume flux feeding a specific single flow unit or group of units, when many more are active within the flow field. It will thus be less than the total effusion rate (Fig. 1b). For clarity the spatial scale of the measurement (point, local, regional or total) should be stated when measurements are presented, as should the temporal scale (instantaneous

effusion rate, time averaged discharge rate, eruption rate or mean output rate).

Bulk versus Dense Rock Equivalent (DRE)

Bulk effusion rates (E_{bulk}) consider the total volume including fluid, solids (crust and crystals) and voids (vesicles and gaps between clinker). Dense rock effusion rates (E_{DRE}) are defined as bulk effusion rates corrected for the vesicle volume fraction (ϖ), i.e. $E_{DRE} = E_{bulk}(1 - \varpi)$. Thus dense rock effusion rates should include only the lava component of the mixture. In the absence of directly measured values for vesicularity, ϖ has been taken from the literature. Rowland et al. (1999), for example, corrected bulk volumes obtained at Kilauea using a void correction of 25% for ′a′a flows (from Wolfe et al. 1988), 60% for near-vent rheomorphic lava and 35% for tube-fed pahoehoe (from Wilmoth and Walker 1993; Cashman et al. 1994). Values for Etnean ′a′a and pahoehoe given by Herd and Pinkerton (1997) and Gaonac'h et al. (1996) are 24±15, or 22±7% if only data within 1 standard deviation of the mean are considered. This, in turn, compares with the findings of Sparks et al. (1998) who corrected volume data for the Soufriere Hills dome material (Montserrat) for a porosity of 8–21%.

Because bulk effusion rates are functions of the lava flux as well its vesicularity, both of which can vary greatly in space and time, changes in the bulk effusion rate may relate to a change in the bubble content, rather than the volume of erupted lava. During the Mauna Loa 1984 eruption, Lipman and Banks (1987) noted down-channel decreases in vesicularity causing a down-channel decrease in bulk volume. This would have caused the bulk effusion rate measured at the vent versus the distal location to be different, but the dense rock values to remain the same, provided that the correct vesicularity was used at each station. Likewise, Madeira et al. (1996) noted that post-eruption degassing of the lava during the 1995 Fogo eruption led to a 10% reduction in the bulk volume.

Variations in E_{DRE} and E_{bulk} may thus have different causes, and therefore different implications. Differences in E_{DRE}, for example, will point to variations in the rate at which lava is being supplied to the measurement point. This, in turn, can be used to make inferences about the mass balance (the balance between volume supplied, intruded and erupted) for a volcano or the pressure conditions in the deep and shallow system (e.g. Allard 1997; Denlinger 1997; Denlinger and Hoblitt 1999; Dvorak and Dzurisin 1993; Dzurisin et al. 1984; Harris et al. 2000). Also, because bulk values may be heavily influenced by the variable presence of vesicles, if we want to compare erupted fluxes at different times during the same eruption, for different eruptions or at different volcanoes, dense rock values must be used.

Being a measure of the variation in fluid flux as well as its vesicularity, bulk effusion rate should be treated with care. If differences are observed between values, the cause of the variation needs to be first isolated, before the meaning or significance of the change can be assessed. However, DRE values must also be treated with care, especially when this value is not obtained directly from lava sampled during the effusion rate measurements, but from a mean vesicularity value taken from literature. In these cases values will have been measured during different eruptions, and maybe for different flow types, and a value appropriate to the case under consideration needs to be used. The vesicularity values for Etnean lavas given in Gaonac'h et al. (1996), for example, range from ~4% for channelized lava to 30% for pahoehoe.

Measurement of effusion rates

The measurement of effusion rates during eruptions has evolved from field-based techniques, see Pinkerton (1993) for a review, to methodologies using geophysical and remote sensing technologies (e.g. Calvari et al. 2005; Harris et al. 1997a,b, 1998, 2006; Kauahikaua et al. 1996; Mazzarini et al. 2005; Rowland et al. 1999; Zebker et al. 1996). We next describe each of the main methods, necessary considerations, the assumptions they make, and the likely errors.

Field-based approaches

Channel-based measurements of instantaneous effusion rate

Instantaneous effusion rate can be obtained by multiplying the mean velocity (V_{mean}) at which lava flows through the cross-sectional area (A) of the channel or pipe within which flow is contained. Cross-sectional area can be calculated from the measured flow depth (d) and/or width (w), either assuming a semi-circular or rectangular channel form (e.g. Barberi et al. 1993; Calvari et al. 1994, 2003; Guest et al. 1987; Harris and Neri 2002; Madeira et al. 1996; Pinkerton 1993; Pinkerton and Sparks 1976; Woodcock and Harris 2005).

In a channel, flow depth can be measured by plunging a piece of iron 're-bar' into the flow and noting the level on that bar (e.g. Calvari et al. 1994; Pinkerton 1993; Pinkerton and Sparks 1976). However, such measurements are impossible when lava channels are very wide, very deep, or flow velocity is high (Pinkerton 1993), although dropping re-bars from helicopters has been attempted in such cases (Lipman and Banks 1987). In addition, at large channels radiant heat from the flow surface can prevent

close approach even when wearing a thermal suit, and the possibility of overflows or levée collapse may add further danger. Lava stiffness coupled with rough levées or thick surface crusts can also impede bar insertion. For flows that are particularly viscous, of high yield strength and/or possessing significant surface crusts, penetrating the surface may prove extremely difficult if not impossible.

Flow depth has also been approximated using the measured height (*H*, Fig. 5) of the channel outer levees (e.g. Calvari et al. 2003; Guest et al. 1987; Pinkerton and Sparks 1976). This assumes that the channel-base is level with the levée bottom. This was found to be a correct assumption in most of the 1999 Etnean flows measured after drainage by Calvari et al. (2003). In other cases the assumption may not hold (e.g. Guest et al. 1987; Pinkerton and Sparks 1976). For example, in cases where mechanical and thermal erosion cause the channel bed to attain a level lower than the levee base, the use of the levee height will lead to an under-estimation of flow depth. On the other hand where flow levels are lower than the levée rim (e.g. Woodcock and Harris 2005), this will lead to an over-estimate (e.g. Figs. 4b and 5). By noting the flow level within the channel during flow a correction can be made (e.g. Bailey et al. 2006).

Flow width can be measured using standard surveying techniques, e.g. tape measure, triangulation, laser range-finder binoculars, etc. Alternatively channel width, as well as levée height, can be obtained from laser altimeter data (e.g. Mazzarini et al. 2005) or from the dimensions on scaled digital visible-light or thermal images (e.g. Bailey et al. 2006; Harris et al. 2004). However, channel width may vary with depth, invalidating the semi-circular or rectangular shape assumption (e.g. Bailey et al. 2006; Guest et al. 1987; Pinkerton 1993). This is most common at channels with overhanging rims, where the resulting channel shape needs to be taken into account in the calculation of the cross-sectional area (e.g. Fig. 4b).

Alternatively, it may be possible to verify channel depth, width and shape after drainage (e.g. Calvari et al. 2003; Harris and Neri 2002). In cases where mapped sections of drained channels are used to obtain cross-sectional area, derived depth may be conservative because it does not take into account un-drained flow material residing on the channel floor. A flow level will also have to be assumed, and brim-full flow is not always the case (e.g. Fig. 4b). In such cases an assumption that the channel was full, so that channel depth equates to flow depth, will result in an over-estimate of effusion rate. Flow level within the channel during flow can be obtained, however, from high-stand and drain-back features following channel drainage, allowing a correction for below-bank flow levels to be made (e.g. Woodcock and Harris 2005).

Flow velocity can be obtained from recording the time taken for distinctive markers in the flow to travel a known distance (Guest et al. 1987; Pinkerton 1993). Flow velocities, however, will vary with depth and width (Frazzetta and Romano 1984; Guest et al. 1987; Pinkerton and Sparks 1976). Velocities will decay horizontally and vertically away from a maximum velocity at the channel centre (Figs. 5 and 6). Thus surface velocity obtained at the flow centre, or the flow margins, is not representative of the mean flow velocity. An added complication is that the crust and core may advance at different velocities causing further vertical velocity variation (e.g. Frazzetta and Romano 1984; Guest et al. 1987). For example, Pinkerton and Sparks (1976) estimated that during the 1975 Etna eruption crusts moved at 0.7 times the velocity of the interior.

Flow velocity is probably easiest to measure at the flow center. At this location the measurement will approximate the maximum flow velocity (Fig. 6). This maximum

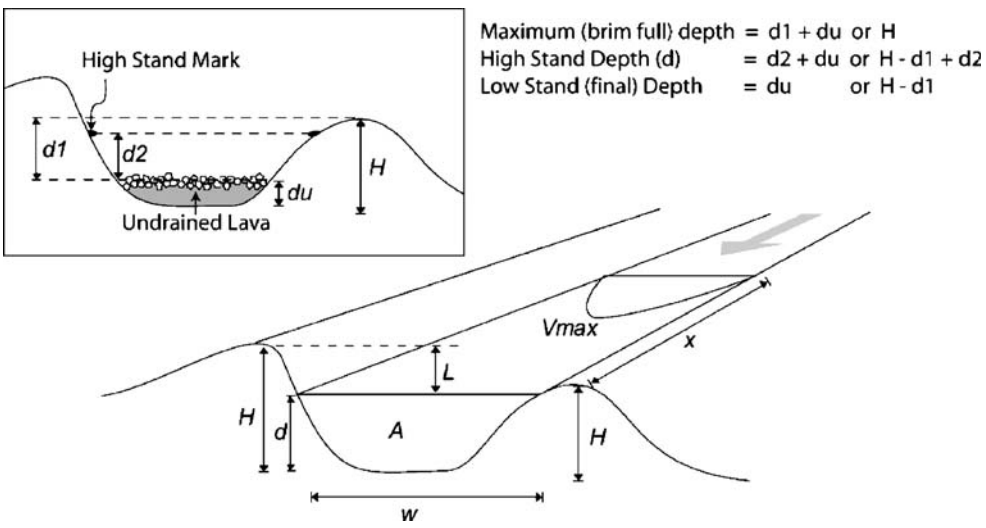

Fig. 5 Summary of parameters required to estimate effusion rate in an active (*main panel*) and inactive, partially drained (*inset*) channel. Notation as follows: A = flow cross-sectional area, d = flow depth, du = depth of un-drained flow, d1+du = depth of brim full flow, d2+du = depth of below bank flow revealed by inner-levee high stand mark, H = levee height, L = flow level below levee rim ($D=H-L$), V_{max}= maximum flow velocity, w= flow width

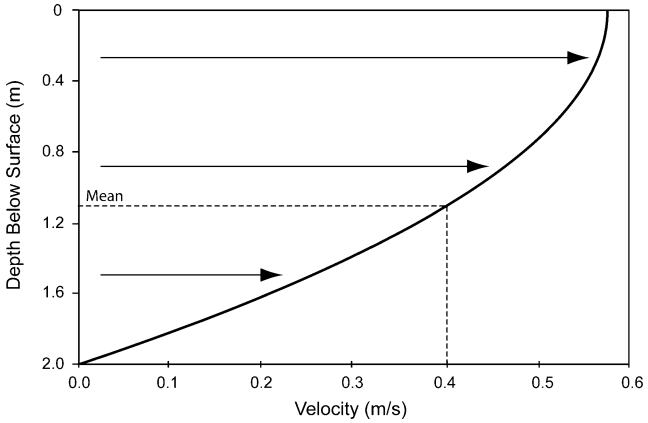

Fig. 6 Velocity profile calculated for a channel of depth 2 m, containing lava with a density of 2,028 kg/m^3 (assuming a dense rock value of 2,600 kg/m^3 and 22% vesicularity) and a viscosity of 3,000 Pa s flowing down a 5° slope. Position of the mean velocity is marked with the *dashed line* and is 67% of the maximum, surface velocity

velocity can then be used to recreate vertical and horizontal velocity profiles for the lava flowing in a channel of known dimensions and with a known or estimated rheology (e.g. Fig. 6). Integrating across these profiles provides one way of obtaining a mean velocity for use in effusion rate calculations (e.g. Dragoni 1989; Dragoni et al. 1986; Fink 1993; Tallarico and Dragoni 1999).

If we calculate the mean velocity for the velocity profile given in Fig. 6, we obtain a mean velocity (v_{mean}) that is 67% of the maximum velocity. Thus, to simplify the problem, the channel cross-section is considered rectangular and mean flow velocity is taken as ~2/3 of the maximum surface velocity, i.e. E_r=0.67 V_{max} d w, as used by Calvari et al. (2003). This is an appropriate approximation for most cases in which the flow is much wider than it is deep.

Model-based measurements

Flow velocity can also be model-calculated using lava density (ρ), acceleration due to gravity (g), channel-floor slope (α) and viscosity (η) in the Jeffreys (1925) equation:

$$v_{mean} = \rho g \sin(\alpha) d^2 / n \eta \quad (1a)$$

in which n is a constant dependant on channel width, values of 3 being used by Booth and Self (1973) for wide channels and 8 for semi-circular channels (Moore 1987). Now, effusion rate (E_r) can be calculated from the measured channel dimensions and underlying slope from:

$$E_r = v_{mean} w d = w \rho g \sin(\alpha) d^3 / n \eta \quad (1b)$$

(e.g. Baloga et al. 1995; Harris and Rowland 2001; Harris and Neri 2002; Jurado-Chichay and Rowland 1995; Keszthelyi and Self 1998; Keszthelyi et al. 2000; Rowland et al. 2003–2005). Effusion rates can also be obtained in this manner by integrating the vertical velocity profile through the entire flow thickness (Dragoni 1989; Dragoni et al. 1986; Fink 1993; Oddone 1910; Tallarico and Dragoni 1999; Soule et al. 2005). In a similar approach, velocity has been calculated by assuming that the velocity for lava flowing around a super-elevated bend can be calculated following Newton's second law of motion, i.e. $v = [r g(\tan \beta)]^{1/2}$, in which r is the radius of curvature and β is the angle of super-elevation (Heslop et al. 1989). Effusion rate is then obtained by multiplying the cross-sectional area of the flow by the velocity (Heslop et al. 1989; Woodcock and Harris 2005). Velocity, and hence effusion rate, has also been obtained from run-up heights (h_{up}) on cones, i.e. from the kinetic energy required to give the run-up height via $v = (2 h_{up} g)^{1/2}$ (Guest et al. 1995).

However, velocities and effusion rates obtained in these ways can sometimes be too high (Kauahikaua et al. 2002; Soule et al. 2004). Over-estimates may result from the assumption of bank-full channel flow in setting a value for depth in Eqs. 1a and 1b. In channels where below-bank-flow was typical, and in which anomalously high levees resulted from construction during short overflow events during rare surges or overflow of volumes backed-up behind blockages (e.g. Bailey et al. 2006; Lipman and Banks 1987), this would cause an over-estimate of the typical volume flux. Soule et al. (2004) also point out that apparent run-up features may instead be high stand marks left by drainage of ponded flow. Use of such features for calculated flow velocities for the 1823 Keaiwa flow of Kilauea may have resulted in a velocity over-estimate by a factor of 5.

Thus, applying Eqs. 1a and 1b to drained-channels requires some assumptions regarding flow depth. Assuming that the channel was filled to the top would give maximum possible flow depth and will yield a maximum value for v_{mean}, and hence E_r. This would give an over-estimate of effusion rates necessary to maintain typical, below-bank flow. Lower flow levels within the channel will reduce d, and hence the derived flow velocities and effusion rates.

As already discussed, channel may have been fed by a range of fluxes, hence leading to a variety of depths. Pulsing or variable flow levels can build characteristic channel forms where a series of thin overflow units of limited spatial extent will be emplaced during the pulse-induced overflows (Bailey et al. 2006). Likewise, variations in the level of flow within the channel can produce high-stand marks on the inner channel wall as well as syn-channel benches, levees and drain-back features such as driblet trains/ridges (e.g. Lipman and Banks 1987; Woodcock and Harris 2005; Figs. 4 and 7). In such cases, use of the brim-full depth will yield maximum effusion rates during the (possibly brief) periods of highest effusion that built the maximum channel depth. Level markers within the channel

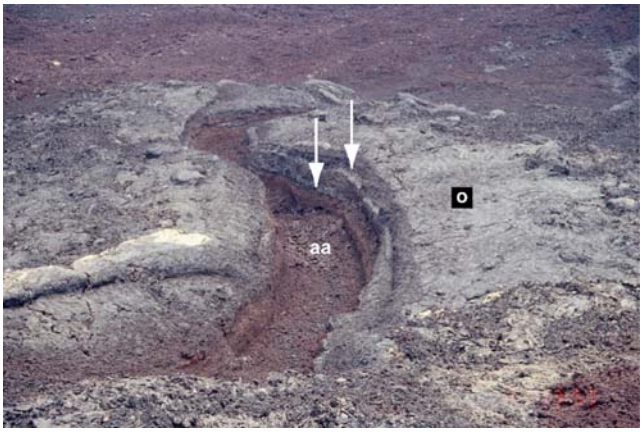

Fig. 7 Inactive channel within the Mauna Ulu 1969–1974 flow field (Kilauea) showing overflow Pahoehoe levées emplaced during pulses (*marked* "o"), and high stand levels (*marked by arrows*) on the inner channel walls, as well as un-drained ′a′a on the channel floor (*marked aa*). While the channel-floor ′a′a marks the lowest observable flow level, the overflow levees mark the highest level. Channel is ~2 m wide

can be used to estimate the lower (possibly more typical) fluxes that fed the channel. In all cases, the depth of un-drained lava on the channel needs to be considered if the full depth is to be obtained (e.g. Fig. 7).

Tube-based measurements

As at channels, for lava tubes problems exist regarding measurements of tube dimensions and flow depth during, as well as after, activity. In addition, the same flow velocity problems apply in the tube as in the channel. These problems are exaggerated by the impossibility of access to a tube during activity, and the unknown, possibly complex, tube shape (e.g. Calvari and Pinkerton 1999). Where a view of the tube-contained lava stream is possible at a skylight, estimates of the stream width and velocity may be possible. The assumption of a semi-circular channel allows cross-sectional area to be estimated. If two skylights are present, velocity may be measured by timing the passage of a marker between the two skylights of known separation distance, as detailed in Tilling and Peterson (1993). The assumptions here are that the tube takes the straight-line course between the two skylights, that the travel of the marker is not impeded by cascades, pools or eddies (Tilling and Peterson 1993; Tilling et al. 1987), and the marker is not detained by drag on the roof or sides of the flow. As a result, this will be a minimum velocity, especially at a meandering tube (Tilling et al. 1987). If no skylights are present, then no velocity (and hence effusion rate) estimate is possible.

Drained tubes allow tube dimensions to be measured after an eruption, allowing for constraint of the tube dimension and shape. As with channel-contained flow, when calculating the flow cross-sectional area, the assumption that the tube flowed full may yield an over-estimate. Tubes may not necessarily flow full (Kauahikaua et al. 1998) and tube dimensions may be increased by thermal and mechanical erosion (e.g. Kauahikaua et al. 1998; Kerr 2001). In these cases, the tube cross-section will become much larger than that of the lava flowing in it. Non-tube-filling-flow levels can, however, be determined from stand-lines along the tube wall, as well as from the level of any un-drained surface within the tube (e.g. Fig. 8).

As with channels, flow velocity can be calculated using Eqs. 1a and 1b, but it is essential to use the correct level. In the Fig. 8a case, for example, assuming that the tube flowed full gives a flow depth of ~2 m. Using this with a viscosity of 100 Pa s and slope 3°, we obtain a mean velocity of 7 m/s. This, given a flow width of 2 m, converts to an effusion rate of 28 m^3/s. However, if we use the flow depth for the two

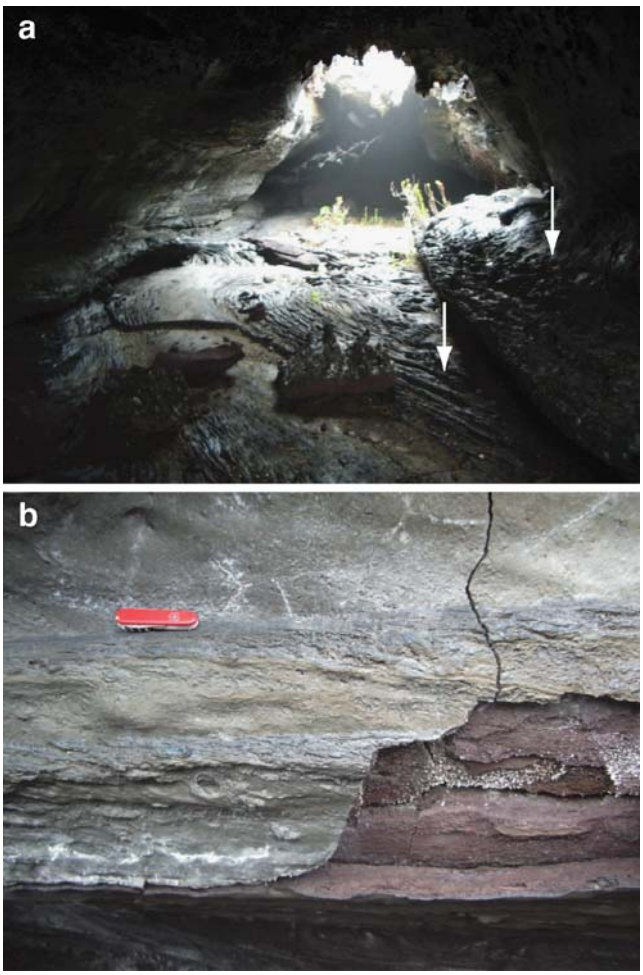

Fig. 8 Lava tubes in the Mauna Ulu 1969–1974 flow field. **a** Shows a ~2 m wide tube section approaching a skylight. On the tube floor an un-drained channel is apparent (*lower arrow*), as well as lateral benches (*upper arrow*). These respectively mark low and moderate lava levels. The distance from the channel surface to the tube roof is ~1.5 m. **b** Shows a thin (~10 cm thick) lava coating veneering a lava tube wall caused by a high flow level, where the level is revealed by the change in surface texture at the level of the pen-knife

lower levels of 0.5–1.0 m then we obtain mean velocities of 0.4–1.7 m/s, and effusion rates of 0.4–3.5 m^3/s. Given that the bulk mean output rate reported during the eruption was ~3 m^3/s (Swanson et al. 1979; Tilling et al. 1987) these latter values seem more reasonable, with the low effusion rate representing a final, late stage flow that remained, undrained, in the tube.

Geophysical approaches

Other ways of obtaining effusion rate from field surveys involve combining one of the methods listed before to calculate flow surface velocity with a measurement of the channel or tube "wet area," i.e. the area of the channel/tube occupied by flowing lava. This can be obtained from geoelectrical, ground penetrating radar or VLF (Very Low Frequency) surveys (e.g. Bozzo et al. 1994; Budetta and Del Negro 1995; Jackson et al. 1987; Kauahikaua et al. 1996; Miyamoto et al. 2005).

Volume-based measurements

This method of obtaining time-averaged discharge rates involves measuring the change in volume of a lava flow or dome over a known period of time. The volume emplaced over the given time interval is then divided by time to obtain the time-averaged discharge rate (e.g. Andronico et al. 2005; Behncke and Neri 2003; Burton et al. 2005; Fink et al. 1990; Harris and Neri 2002; Mazzarini et al. 2005; Nakada and Fujii 1993; Nakada et al. 1999; Richter et al. 1970; Rose 1972; Rossi 1997; Rowland et al. 1999; Sparks et al. 1998; Swanson and Holcomb 1990; Wolfe et al. 1988; Zebker et al. 1996).

One quick and relatively simple means of gaining regular volume measurements at known time intervals is to measure the area of newly emplaced lava, and to multiply this by a mean thickness estimated from field measurements (e.g. Andronico et al. 2005; Behncke and Neri 2003; Mazzarini et al. 2005; Pinkerton and Sparks 1976; Rossi 1997; Zebker et al. 1996). Repeat (daily or weekly) measurements of any new lava flow areas allow the flow volumes erupted over these periods to be estimated. A rapid means of measuring the flow area is by walking or flying around the flow perimeter carrying a continuously recording GPS. Dividing the resulting volume by the emplacement time allows calculation of time averaged discharge rate, averaged over the time frame of a few hours to days. This approach provided the discharge data given in Fig. 2. For this calculation to be suitable, the emplacement time of the flow must be well known, many measurements of flow thickness need to be obtained along the flow margins, and the edge thickness must be representative of the lava body as a whole.

If significant thickening occurs away from the edges, an error will result from the assumption that lava thicknesses measured at the flow edge are typical across the entire flow field. This may induce large errors for complex flow fields emplaced over long periods of time, i.e. in cases where thick piles of lava can develop within the flow field. For example, if we take the mean edge thickness of 3–10 m for the 1991–1993 Etna lava flow field and multiply by the area (7.2 km^2) we obtain a volume of $22–72\times10^6$ m^3. This is significantly smaller than the actual volume of $231\pm29\times10^6$ m^3 due to substantial thickening by up to 96 m (with a mean of 32 m) away from the flow field edges (Stevens et al. 1997).

Where accurate pre-, syn- or post-eruption Digital Elevation Models (DEMs) are available, measurements of the flow volume can be obtained from DEM subtraction. Given the duration of lava flow activity between the two DEM-derived volumes time-averaged discharge rate can be obtained by dividing the residual volume by time. Based on an estimated flow thickness of 3 m and an area of 8.2 km^2, Rowland (1996) estimated a DRE volume of 0.02 km^3 for the 1995 flow field of Fernandina. Rowland et al. (2003), however, were able to measure pre- and post-eruption topography for all locations across the flow, resulting in a revised, more accurate, volume of 0.04 km^3. The relative error between two DEMs can also lead to significant error in the volume calculation.

Other methods to estimate flow volumes, and hence time-averaged discharge rates and mean output rates, include:

1. Generation of DEMs using digitised cartographic map data (Stevens et al. 1999).
2. Use of volumes erupted into, and thereby contained within, pit craters of known volume (Jackson et al. 1975; Richter et al. 1970; Rowland and Munro 1993).
3. Repeat GPS-located laser-range finder measurements onto an active dome or flow, and/or levelling measurements, plus use of maps, photographs, triangulation and photogrammetry (Nakada and Fujii 1993; Nakada et al. 1999; Rose 1972; Rowland and Munro 1993; Sparks et al. 1998).
4. Use of satellite optical or thermal data (Stevens et al. 1997; Patrick et al. 2003), laser altimeter (Mazzarini et al. 2005) and/or interferometric radar data (Rowland 1996; Rowland et al. 1999, 2003; Zebker et al. 1996) to obtain flow area and thickness, and hence volume by integrating thickness over the area (e.g. Patrick et al. 2003).

Methodologies, issues, problems, and errors for these volume measurement techniques are considered in each of the cited studies, where some of the general considerations detailed here apply to all data sets.

Sulphur flux based measurements

The petrographic method of Devine et al. (1984) estimates sulfur loss from a magma by comparing the concentration of sulfur in pre-eruption melt inclusions with that in post-eruption glasses. Using this value of sulfur loss during degassing, the volume of magma required to give a measured sulfur dioxide (SO_2) flux can be calculated (e.g. Allard et al. 1994; Andres et al. 1989, 1991; Greenland et al. 1988; Kazahaya et al. 1994; Stoiber et al. 1986; Sutton et al. 2001, 2003). In addition, Kazahaya et al. (1994) show how mass rates of magma degassing M (in kg/s) can be obtained from the emission rates of magmatic water (Q_{H20}), as well as SO_2 (Q_{SO2}), in:

$$M = 10^2 Q_{H20} / \Delta C_{H20} \quad (2a)$$

or

$$M_{SO2} = 10^6 M_S Q_{SO2} / M_{SO2} \Delta C_S \quad (2b)$$

in which ΔC_{H20} and ΔC_S are the decrease in water and sulfur content (wt.%) of magma during degassing, and M_S and M_{SO2} are the molecular weights of sulfur and SO_2. Given the average basaltic andesite sulfur loss (0.0495 wt.% Sulfur) and measured SO_2 emission rates at Lascar (2,300± 1,120 Mg/d) during 1989, Andres et al. (1991) calculated a degassed magma volume flux of 9.3×10^5 m^3/d.

If all degassed magma is then erupted, these degassed volume fluxes will equate to effusion rates. Sutton et al. (2003) detail this technique for assessing daily discharge rates from SO_2 fluxes for the Kupaianaha—Pu'u 'O'o eruption of Kilauea, where comparisons with VLF-derived rates were in good agreement. However, this technique will provide an under-estimate for the discharge rate if previously degassed magma is erupted (e.g. Burton et al. 2005) or an over-estimate if not all of the degassed magma is erupted (e.g. Andres et al. 1991). At Lascar, for example, the degassed volume of 9.3×10^5 m^3/d calculated by Andres et al. (1991) compared with a two orders of magnitude smaller time averaged-discharge rate for the extruded volume forming the Lascar lava dome of 6.3×10^3 m^3/d.

Use of deformation data

Volumes leaving shallow storage areas to contribute erupted lava can be estimated from deflation as revealed by, for example, tilt measurements (e.g. Rowland and Munro 1993; Tilling 1987; Tilling et al. 1987; Tryggvason 1986) or synthetic aperture radar (e.g. Fukushima et al. 2005; Lu et al. 2005; Massonnet et al. 1995). Complications resulting from the dynamic balance between supply to the shallow system and drainage of that system complicate any assumption that the volume of deflation equates to the erupted volume (e.g. Denlinger 1997; Dvorak and Dzurisin 1993; Dzurisin et al. 1984). A significant portion of the volume leaving the shallow system may, for example, be intruded as well as extruded (e.g. Bjornsson et al. 1977; Denlinger 1997; Dvorak and Dzurisin 1993; Dzurisin et al. 1984; Harris et al. 2000; Tryggvason 1986). These and other complications, e.g. source shape, sub-surface structure and material property assumptions (e.g. Lu et al. 2005) mean that erupted volumes do not always equate to measured volumes of deflation (Fukushima et al. 2005; Lu et al. 2005; Massonnet et al. 1995).

Seismic approaches

Battaglia et al. (2005) present a method to estimate effusion rates from seismic amplitudes, using either the tremor source amplitude or squared amplitude at any point in time. This was calibrated using data from the 1998 eruption of Piton de la Fournaise, and tested using data from three other eruptions. Results showed that the use of amplitude in the 5–10 Hz bands over-estimated the lava volume, possibly due to the signal being not directly generated by magma flow but by gas flow. For two of the three eruptions, however, lava volumes obtained using bands below 5 Hz were ~30% lower than field measured volumes, although field measurements themselves may have been over-estimated (Battaglia et al. 2005).

Thermal approach

The thermal methodology for obtaining effusion rates is based on the work of Pieri and Baloga (1986) and Crisp and Baloga (1990). It was adapted to satellite thermal data by Harris et al. (1997a,b) and has since been developed using thermal data obtained for active lava areas from a variety of satellite based sensors (Table 1) as well as ground-based thermal imagers (Calvari et al. 2005; Harris et al. 2006).

The thermal method is based on a simple heat budget for an active lava flow in which all heat supplied to the active flow unit (Q_{in}) is lost from the flow surfaces (Q_{out}), so that $Q_{in} = Q_{out}$ (Crisp and Baloga 1990; Harris et al. 1997a; Pieri and Baloga 1986). Heat is supplied by advection (Q_{adv}) and crystallization (Q_{cryst}) during cooling between eruption temperature and solidus (δT), i.e. $Q_{in} = Q_{adv} + Q_{cryst}$. While heat losses from the flow surface are radiation (Q_{rad}) and convection (Q_{conv}), heat loss by conduction (Q_{cond}) will also occur through the flow base. Thus $Q_{out} = Q_{rad} + Q_{conv} + Q_{cond}$ (Harris and Rowland 2001; Harris et al. 1998, 2005; Keszthelyi and Self 1998; Keszthelyi et al. 2000).

Table 1 Application and development of the thermal approach to extract lava discharge rates, showing the range of eruption types, data and lava surface temperature assumptions used to calculate active lava area, and hence heat flux (Eqs. 3–4)

Volcano	Eruption/years	Eruption type / effusive or extrusive style	Data	Assumed T_{surf} range (°C)	Reference
Ascraeus Mons	Planetary	Channelized martian flow	Heat loss model	Calculated	Crisp and Baloga (1990)
Bezymianny	2000	Lava dome	AVHRR, MODIS	100–500	Steffke (2005)
Erebus	1985 & 1989	Lava lake	TM	Not assumed	Harris et al. (1999a)
Erebus	1980	Lava lake	AVHRR	578–715	Harris et al. (1999b)
Erta Ale	1986	Lava lake	TM	Not assumed	Harris et al. (1999a)
Etna	1991–1993	Flank eruption (channel & tube fed ′a′a)	AVHRR	100–500	Harris et al. (1997a)
Etna	1980–1999[a]	Flank & summit eruptions (channel & tube fed ′a′a)	AVHRR, ATSR, TM	100–500	Harris et al. (2000)
Etna	November 1999	Fountain-fed (channel fed ′a′a)	AVHRR, ETM+	100–1000	Harris and Neri (2002)
Etna	2001[b]	Summit & flank eruption (channel & tube fed ′a′a)	AVHRR	100–1000	Lautze et al. (2004)
Fernandina	1995	Flank eruption (channel fed ′a′a)	ATSR	75–500	Rowland et al. (2003)
Kilauea	1991	Tube-fed Pahoehoe	AVHRR & TM	100–500	Harris et al. (1998)
Kilauea	1991	Lava lake (Pu′u ′O′o)	TM	Not assumed	Harris et al. (1999a)
Krafla	1980–1984[c]	Fissure eruptions (fountain & channel fed ′a′a)	AVHRR	97–425	Harris et al. (2000)
Mt. Cleveland	2001	′A′a lava flow down the flanks of a stratocone	AVHRR	100–500	Smith (2005)
Nyiragongo	1987	Lava lake	TM	Not assumed	Harris et al. (1999a)
Okmok	1997	′A′a lava flow (some of it ponded)	AVHRR	100–500	Patrick et al. (2003)
Santiaguito	1987–2000	Dome & silicic lava flow extrusion	TM & ETM+	Not assumed	Harris et al. (2003)
Santiaguito	2000	Silicic lava flow extrusion	ETM+	Not assumed	Harris and Neri (2002)
Santiaguito	2000–2002	Silicic lava flow extrusion	TM & ETM+	Not assumed	Harris et al. (2004)
Stromboli	1985–1986	Flank eruption (channel & tube fed ′a′a)	AVHRR	100–500	Harris et al. (2000)
Stromboli	2002–2003	Flank eruption (channel & tube fed ′a′a)	AVHRR, MODIS	100–1,000	Calvari et al. (2005)
Stromboli	2002–2003	Flank eruption (channel & tube fed ′a′a)	FLIR	Not assumed	Harris et al. (2006)

Acronyms used are: *AVHRR* (Advanced Very High Resolution Radiometer), *ATSR* (Along Track Scanning Radiometer), *TM* (Thematic Mapper), *ETM+*(Enhanced Thematic Mapper Plus) and *FLIR* (Forward Looking Infrared Radiometer)

[a] March 1981, February 1981, 1983, 1984, March–July 1985, December 1985, 1986–87, September 1989, September–October 1989, 1991–1993, 1996, and 1999 eruptions

[b] January–July SE Crater eruption and July–August S. Flank eruption

[c] July 1980, October 1980, January–February 1981 and 1984 eruptions.

For simplicity, we assume that Q_{out} is dominated by the surface heat losses. These are defined by:

$$Q_{rad} = A\varepsilon\sigma\left(T_{surf}^4 - T_{amb}^4\right) \quad (3)$$

$$Q_{conv} = Ah_c(T_{surf} - T_{amb}) \quad (4)$$

In which A and T_{surf} are the area and surface temperature of the active flow, T_{amb} is the ambient temperature, and ε, σ and h_c are the surface emissivity, the Stefan Boltzmann constant and the convective heat transfer coefficients. Heat supplied by advection and crystallization in cooling through δT can be described by:

$$Q_{adv} = E_r \rho c_p \delta T \quad (5)$$

$$Q_{cryst} = E_r \rho \phi c_L \quad (6)$$

in which E_r, ρ, c_p, ϕ and c_L are the discharge rate, lava density, specific heat capacity, crystallisation in cooling through δT, and latent heat of crystallisation of lava,

respectively. The two heat supply terms have discharge rate in common so that $Q_{out} = Q_{in}$ can be written

$$Q_{rad} + Q_{conv} = E_r \rho \left(c_p \delta T + \phi c_L \right) \quad (7)$$

Rearranging allows calculation of E_r from

$$E_r = \left(Q_{rad} + Q_{conv} \right) / \rho \left(c_p \delta T + \phi c_L \right) \quad (8)$$

Given that this method takes into account the volume flux necessary to account for cooling over a given time, this will yield time-averaged discharge rate (Wright et al. 2001a). In all the cases given in Table 1, measured values for Q_{rad} and Q_{conv} are used with assumed values for ρ, c_p, δT, ϕ and c_L. Assumed values for ρ, c_p, and ϕ differ by case, for example, post eruption crystallization is different for Etna and Kilauea, and differing vesicularities will cause bulk values for ρ and c_p to vary (Table 2). Harris et al. (2000) provide a sensitivity analysis for the effect of varying each of the assumed values in Eq. 8 on calculated E_r.

Satellite-based methodology

Calculation of Q_{rad} and Q_{conv} have generally been obtained from satellite data (e.g. Oppenheimer 1991; Oppenheimer et al. 1993; Harris et al. 1997a,b, 1998). In many cases a value, or range of values, for the surface temperature of the active flows is assumed in order to extract active flow area. In most cases, active lava flow areas have been obtained from Advanced Very High Resolution Radiometer (AVHRR) or Thematic Mapper (TM) data using an assumed range of reasonable surface temperatures to obtain surface area. This involved modeling a pixel containing lava at an assumed temperature (T_{surf}) surrounded by ambient ground at a known temperature (T_{back}). Now the pixel portion occupied by active lava (p) can be calculated, using the pixel integrated temperature (T_{int}) in the following mixture model (Dozier 1981; Harris et al. 1997a, 1999a; Matson and Dozier 1981; Oppenheimer et al. 1993; Rothery et al. 1988):

$$L(\lambda, T_{int}) = pL(\lambda, T_{surf}) + (1 - p)L(\lambda, T_{back}) \quad (9)$$

in which L is the Planck function for a blackbody at wavelength λ.

If p (i.e. lava area) is known, Eq. 9 can be solved for T_{surf} (Dehn et al. 2002). Similarly a range of 100–1,000°C has been assigned for T_{surf} to solve for p (Table 1). In this case, the only variable in Eqs. 3 and 4 becomes A; T_{surf}, σ, h_c and T_{amb} either being constant or assumed (Table 2). As pointed out by Wright et al. (2001a), in such a case all the assumptions causes Eq. 8 to reduce to:

$$E_r = mA / c \quad (10)$$

which can be further reduced to $E_r = x\,A$, in which $x = m/c$, m and c being the coefficients that define a direct relationship between time-averaged DRE discharge rate and active lava flow area. The coefficients m and c are, respectively, defined by the values assumed for the heat loss and heat supply models:

$$m = \sigma \left(T_{surf}^4 - T_{surf}^4 \right) + h_c \left(T_{surf} - T_{amb} \right) \quad (11)$$

$$c = \rho \left(c_p \, \delta T + \phi c_L \right) \quad (12)$$

Table 2 Values used to calibrate the thermal approach at Kilauea (Harris et al. 1998), Etna (Harris et al. 2000), Krafla (Harris et al. 2000), Stromboli (Calvari et al. 2005) and Santiaguito (Harris et al. 2002, 2003) with resultant m, c and x values

Parameter	Kilauea	Etna	Krafla	Stromboli	Santiaguito
T_{surf} (°C)	100–500	100–500	100–500	100–500	125–250
T_{amb} (°C)	35	0	0	0	20
σ (W m^{-2} K^{-4})	5.67×10^{-8}	5.67×10^{-8}	5.67×10^{-8}	5.67×10^{-8}	5.67×10^{-8}
H_c (W m^{-2}K^{-1})	0	~10	~10	~10	35–75
DRE ρ (kg m^{-3})	2,600±100	2,600	2,600	2,600	2,600
DRE c_p (J kg^{-1} K^{-1})	1,225	1,150	1,150	1,150	1,150
Vesicularity (%)	10–40	10–34	10–34	10–22	10–30
Bulk ρ (kg m^{-3})	1,560–2,340	1,720–2,340	1,720–2,340	2,030–2,340	1,820–2,340
Bulk c_p (J kg^{-1} K^{-1})	735–1,100	810–1,035	810–1,035	900–1,035	805–1,035
Cooling range (K)	315–385	200–350	200–350	200–350	200–330
ϕ (%)	2–45	45	45	45	0–45
C_L (J kg^{-1})	3.5×10^5	3.5×10^5	3.5×10^5	3.5×10^5	3.5×10^5
m ($\times10^3$ W m^{-2})	0.8–20	1.8–25	1.8–25	1.8–25	10–13
C ($\times10^8$ J m^{-3})	8.3–6.9	8.8–7.6	8.8–7.6	8.8–9.6	12–2.9
X ($\times10^{-6}$ m s^{-1})	0.9–29	2.1–33	2.1–33	2.1–26	8.5–44

Moving across the table from basaltic to silicic flows, the latter typically have lower surface temperatures than the former (Harris et al. 2002). Note, also for Kilauea assumed post-eruption crystallization rates are the lowest and the range of vesicularities the highest. As a result x increases to the right across the table, where increasing x means that to cover a given area a higher discharge rate will be required.

so that

$$x = m/c = \left[\sigma\left(T_{surf}{}^4 - T_{amb}{}^4\right) + h_c\left(T_{surf} - T_{amb}\right)\right] / \left[\rho\left(c_p \delta T + \phi c_L\right)\right] \quad (13)$$

As long as appropriate values are used in setting x, reasonable discharge rates should be obtained from $E_r = x\,A$. In solving Eq. 13 the most contentious, or difficult to set values are h_c, T_{surf} and δT. These have been set on a case-by-case basis to suit the eruption conditions (lava temperature, crystallinity, vesicularity, etc.) appropriate for each one. Published values used during application of this approach using satellite data for lava flows and domes at Kilauea, Etna, Krafla, Stromboli and Santiaguito are given in Table 2.

To illustrate the application of this approach, the combinations of values used by Harris and Neri (2002) to extract time-averaged discharge rates from AVHRR data for the October–November 1999 eruption of the Bocca Nuova (Etna) are given in Table 3. Each of these models was used to provide a range of time-averaged discharge rates, taking into account the full range of uncertainty in the assumed values. Results can be compared with the time-averaged discharge rates obtained from daily mapping of the flow area and thickness using hand-held and helicopter flown GPS. For this case, the range of discharge rates obtained from the ground-based and satellite-based approaches have uncertainties of 18 and 50%, respectively. However, the two data sets show excellent consistency revealing the same temporal trends, with the ground-based estimates having a narrower range of uncertainty, but typically falling with the satellite-based range (Fig. 9). Generally, time-averaged discharge rates simultaneously measured on the ground and from satellite-sources show reasonable agreement (Table 4; Fig. 10), indicating that the assumed values for each case have provided an appropriate value for Eq. 13.

By combining and re-arranging the equations that comprise the heat budget for an active lava flow we can draw a direct link between time-averaged discharge rate and active lava flow area (Eqs. 9, 10, 11, and 12). Thus, in agreement with Pieri and Baloga (1986), the satellite-based technique has assumed a linear relationship between time-averaged discharge rate and active lava flow area (Wright et al. 2001a). This has involved defining the linear proportionality relationship that Pieri and Baloga (1986) suggested could be formulated between discharge rate and flow area using the typical thermal parameters for an active lava flow. This relationship is defined by the lava heat loss properties, which are mostly controlled by surface temperature, and the heat supply properties. In effect the underlying assumption

Table 3 Values used to calibrate the thermal approach at Etna using AVHRR data obtained during 1999–2002, and following the values and thermal models given in Harris and Neri (2002)

Parameter	Cool model	Hot model (1)	Hot model (2)	Hot model (3)
T_{surf} (°C)	100	500	700	1,000
T_{amb} (°C)	0	0	0	0
σ (W m^{-2} K^{-4})	5.67×10^{-8}	5.67×10^{-8}	5.67×10^{-8}	5.67×10^{-8}
H_c (W m^{-2} K^{-1})	5	9	10	11
Q_{cond} (W m^{-2})	545	6,550	6,550	6,550
A (m^2)	Maximum	Moderate	Moderate	Minimum
DRE ρ (kg m^{-3})	2,600	2,600	2,600	2,600
DRE c_p (J kg^{-1} K^{-1})	1,225	1,225	1,225	1,225
Vesicularity (%)	10	22	22	22
Bulk ρ (kg m^{-3})	2,340	2,020	2,020	2,020
Bulk c_p (J kg^{-1} K^{-1})	1,100	955	955	955
Cooling range (K)	200	350	350	350
ϕ (%)	45	45	45	45
C_L (J kg^{-1})	3.5×10^5	3.5×10^5	3.5×10^5	3.5×10^5
M ($\times10^3$ W m^{-2})	1.8	31	64	167
C ($\times10^8$ J m^{-3})	8.9	10	10	10
X ($\times10^{-6}$ m s^{-1})	2.1	31	64	167

Active flow area (A) is extracted from the satellite data using the relevant, assumed, T_{surf} in Eq. 8. It is then used with the corresponding values given for each model to estimate effusion rate from $E_r = x\,A$. Thus, a lower x value is used with the large flow area extracted for the cool model case (T_{surf} = 100°C), than for the hot models (T_{surf} = 500–1,000°C). Parameter m, in this case considers conduction through the flow base (Q_{cond}), so that Eq. 10 is $m = \sigma\left(T_{surf}^4 - T_{amb}^4\right) + h_c\left(T_{surf} - T_{amb}\right) + Q_{cond}$. Q_{cond} is calculated following Fouriers Law where heat is conducted over a thermal boundary layer (the basal crust) of thickness h that separates the hot core at T_{core} from the cooler, underlying surface at T_{base}. Thus $Q_{cond} = k[(T_{core} - T_{base})/h]$, in which k is thermal conductivity of vesicular basalt. Following Harris et al. (2000), Q_{cond} is set, for the cool model, using k, T_{core}, T_{base} and h of 3 W m^{-1} K^{-1}, 1,100°C, 580°C and 3 m. For the hot model values of 2.5 W m^{-1} K^{-1}, 1,100°C, 580°C and 0.1 m are used.

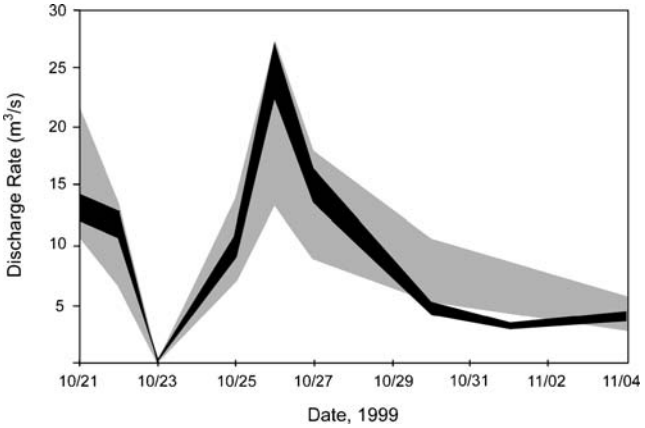

Fig. 9 Range of lava discharge rate calculated using the thermal approach with AVHRR data (*grey zone*) and ground-based approaches (*black zone*) during the 1999 eruption of the Bocca Nouva (Etna). Range of satellite based estimated is obtained using the range of x values given in Table 3. The ground-based range is obtained from measuring flow area emplaced over a known time period, multiplying by a thickness of 2.5–3.0 m and dividing by emplacement duration

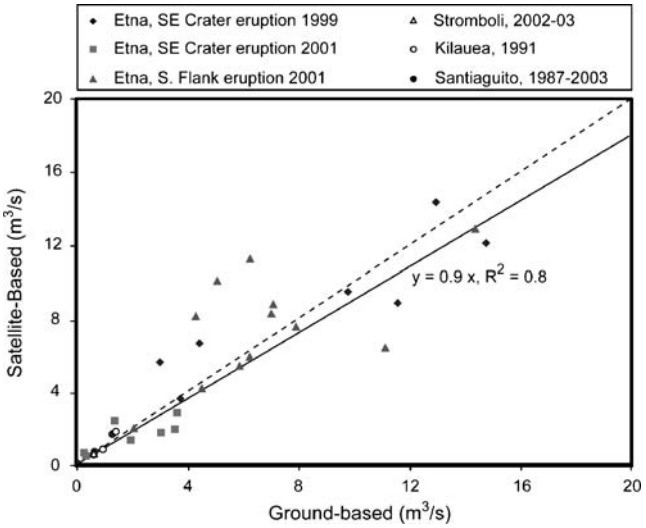

Fig. 10 Comparison of same day satellite-based (thermally-derived) and ground-derived discharge rates. In each case, the mid-point of each measurement range is plotted. A slight difference between the 45° line (*dashed-line*), the line along which all points should fall if there were perfect agreement, and the actual trend of the best fit (*solid-line*) between the two data sets is apparent. This shows that the satellite-based approach provides a range of discharge rates with mid-points that are slightly higher than the ground-based range. Etna data are from Calvari and Harris (unpublished data), Stromboli from Harris et al. (2006), Kilauea from Harris et al. (1998), and Santiaguito from Harris et al. (2003, 2004)

is that the potential area covered by a lava flow at any given effusion rate is cooling-limited (Guest et al. 1987). It will thus fail if the flow is volume or topographically limited (Patrick et al. 2003). Such problems and sources of error due to the assumptions involved in obtaining area from the satellite data are reviewed in Harris and Neri (2002) and Patrick et al. (2003). Thus, in cases where this approach has been applied, a linear relationship between discharge rate and active lava flow area has, in effect, been forced upon the data (Fig. 11). However, setting the x value appropriate to the volcano, eruption or topographic conditions, the good fit with independent ground data indicates that the approach is generally valid.

FLIR-based methodology

Acquisition of thermal data using hand-held imagers allows thermal images of high spatial resolution and dynamic range to be collected. At Stromboli thermal images of the active flow field with a spatial resolution of ~2 m were collected on a near-daily basis during the 2002–2003 effusive eruption to support routine monitoring (Calvari et al. 2005). Given detailed, unsaturated temperature data for the active flow surface, heat losses were calculated on a pixel-by-pixel basis. Discharge rates were then calculated by summing the heat loss obtained for each lava pixel and applying Eq. 8. This methodology, including issues regarding identification of active lava pixels, is detailed in Harris et al. (2006). In this case, both flow area and temperature are variable such that effusion rate is now not just a function of flow area, but also temperature. However,

Table 4 Published comparisons of field-based instantaneous effusion rates and thermally-derived time-averaged discharge rates for cases where near-simultaneous measurements have been possible

Case	Ground-based method	Thermal data	Ground-derived value ($m^3\ s^{-1}$)	Thermally-derived value ($m^3\ s^{-1}$)	Source
Kilauea, (23 July 1991)	VLF[a]	ETM+	1.36±0.14	1.76±0.27	Harris et al. (1998)
Kilauea, (11 October 1991)	VLF[a]	ETM+	0.89±0.09	0.78±0.27	Harris et al. (1998)
Etna (20 April 1983)	Channel-based	AVHRR	14.3±3.0	11.4±1.4	Harris et al. (2000)
Etna (25 April 1983)	Channel-based	AVHRR	28.1±8.5	24.9±5.1	Harris et al. (2000)
Etna (27 April 1983)	Channel-based	AVHRR	20.4±6.8	9.3±2.8	Harris et al. (2000)
Etna (23 June 1983)	Channel-based	AVHRR	2.6±0.5	3.5±1.3	Harris et al. (2000)
Santiaguito (23 January 2000)	Channel-based	ETM+	0.48±0.17	0.48±0.09	Harris et al. (2003)
Stromboli (31 May 2003)	Channel-based	FLIR	0.85±0.75	0.55±0.35	Harris et al. (2006)

[a] Following the method of Kauahikaua et al. (1996)

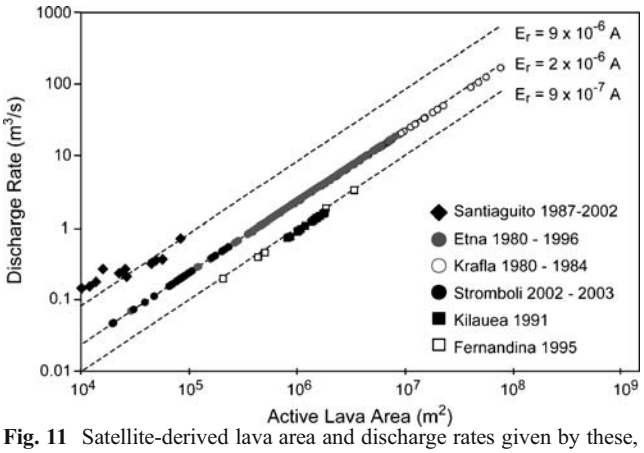

Fig. 11 Satellite-derived lava area and discharge rates given by these, revealing the forced linear relationship between active lava area and discharge rate. Data are from Harris et al. (2000) (for Etna, 1980–1999 eruptions), Harris et al. (1998) (for Kilauea, 1991), Calvari et al. (2005) (for Stromboli, 2002–2003), Harris et al. (2003, 2004) (for Santiaguito, 1986–2003) and Rowland et al. (2003) (for Fernandina's, 1995). For clarity, only the relationships obtained for the minimum x value given in Table 2 are plotted

area is still one of the two variables used to calculate discharge rate. The same applies for ground-based approaches where time-averaged discharge rate obtained from mapping the flow area emplaced in a known time, multiplying by average thickness, and dividing by emplacement duration. In this case area is still one of the two variables used to calculate discharge rate. In these cases, a linear relationship between discharge rate and flow area and temperature, or between discharge rate and flow area and thickness, will be forced. Thus, these data also show a positive linear relationship between discharge rate and active lava area (Fig. 12). The best fit to this relationship implies an x value (in $E_r = x\,A$) in the vicinity of 20–40 $\times$ 10^{-6} m/s.

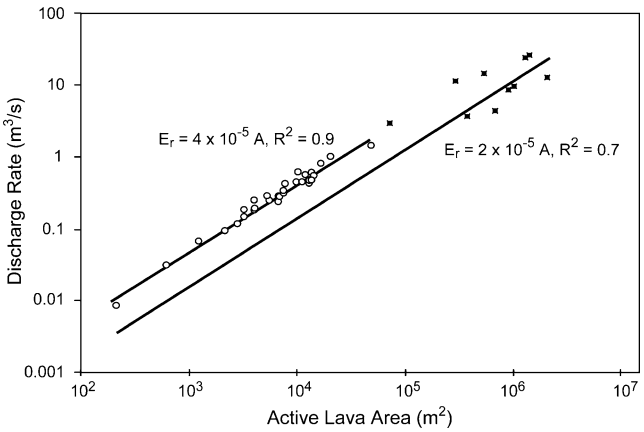

Fig. 12 Discharge rate versus active lava flow area for Stromboli (2002–2003, *white circles*) derived by applying the thermal approach to FLIR data (Harris et al. 2006) and Etna (Bocca Nuova, 1999, *black squares*) using daily measurements of flow area and thickness (Harris and Neri 2002)

Use for hazard monitoring: a case study from Mount Etna

The main threat from volcanic activity on Etna is posed by effusion of lava flows either from the summit craters or from fissures on the lower flanks (Guest and Murray 1979). During the past 25 years damage to buildings, infrastructure, and cultivated areas occurred during the 1981, 1983, 1991–1993, 2001, and 2002–2003 eruptions. The 1981 eruption from vents between 1,800 and 2,250 m on the north–east flank, sent flows towards Randazzo (population 11,200) causing $10 million of damage (McClelland et al. 1989). The eruptions of 1983, 2001 and 2002–2003 caused significant damage to south flank ski facilities (Andronico et al. 2005; Barberi et al. 1993, 2003; Frazzetta and Romano 1984) and posed a threat to Nicolosi, a town of population 6,200 on the south flank. The 1991–1993 eruption posed a significant hazard to Zafferana Etnea (population 8,100), requiring lava diversion to protect the town (Barberi et al. 1993). The 2002–2003 eruption destroyed the north flank ski-complex, damaged that of the south flank (Andronico et al. 2005), and posed a potential threat to the north flank town of Linguaglossa (population 5,300). Opening of vents at low elevations on the flanks of the volcano poses greater hazard due to the higher concentration of towns and villages at these elevations, as well as intensive agriculture, particularly below the 1,000 m elevation. Eruptions from low-elevation vents in 1669 and 1928, respectively, damaged numerous towns, including portions of the city of Catania (Crisci et al. 2003), and the town of Mascali (Chester et al. 1999; Duncan et al. 1996).

Measurement of effusion rate can play a role in assessing the likely hazard posed by an active flow. Peak effusion rate has been shown to play a role in determining maximum flow length (Pinkerton and Wilson 1994; Walker 1973). On Etna there also appears to be an inverse relationship between vent elevation and maximum effusion rate (Wadge et al. 1994). It is thus a critical parameter when considering for maximum lava flow run-out distance and hazard (Calvari and Pinkerton 1998; Kilburn 1996, 2000, 2004; Rowland et al. 2005). Application of empirical formulas designed to relate maximum flow length to effusion rate can provide a good approximation for potential extension of channel-fed single flow units (Calvari and Pinkerton 1998; Kilburn 2000; Pinkerton and Wilson 1994). Such relationships have been extensively used on Etna for rapid hazard evaluation for civil protection purposes during on-going eruptive crises. In such cases, preliminary estimation of the maximum distance that a flow may reach, given the current instantaneous effusion rate, is required in a timely fashion. Use of finite element and thermo-rheological models also

allow likely inundation zones to be assessed (e.g. Costa and Macedonio 2005; Crisci et al. 2003, 2004; Favalli et al. 2005; Harris and Rowland 2001; Ishihara et al. 1990; Wadge et al. 1994).

Complications occur when prolonged lava supply produces long-lived compound flow fields, often fed by complex tube systems. In these cases, insulation of lava flowing in tubes greatly reduces cooling rates and thus increases the cooling-limited distance that a flow can extend at a given effusion rate (Keszthelyi 1995; Keszthelyi and Self 1998). In such cases final flow lengths can be much longer than expected (Calvari and Pinkerton 1998; Kauahikaua et al. 1998; Pinkerton and Wilson 1994). It is, however, very difficult to model and predict lava tube development because tube formation depends on a number of stochastic variables, including stability and duration of lava supply from the source (Calvari and Pinkerton 1998; Kauahikaua et al. 1998). Unfortunately, the influence of these parameters on the final size of a flow field cannot be stated a priori. One way to promptly evaluate the effect of lava tubes in increasing the maximum extent of a lava flow is through frequent thermal mapping (e.g. Andronico et al. 2005; Burton et al. 2005), which allows detailed mapping of tubes and new breakouts (Kauahikaua et al. 2003). In these cases, new breakouts from the exits of lava tubes can be recognised as first-order ephemeral vents (Calvari and Pinkerton 1998) and used as source-vents of new arterial flows for successive simulations.

Direct field measurements of instantaneous effusion rate throughout eruptions at Etna are often difficult (Bailey et al. 2006; Behncke and Neri 2003; Calvari et al. 1994, 2003; Frazzetta and Romano 1984; Harris and Neri 2002; Pinkerton and Sparks 1976). Field surveys are challenging during initial phases of an eruption when effusion rate is a maximum, lava flows are expanding at high speed, and strong explosions, fountaining and lava spattering are occurring at the master vent (Pinkerton 1993). Also, measurements are difficult during more complex events when the eruptive fissure system is extremely long and lava output takes place from a number of different vents to feed multiple flows spread across a large area, such as during Etna's 2001 flank eruption (Behncke and Neri 2003; Calvari and INGV-Catania 2001). In all these cases, the synoptic view afforded by satellite-based sensors has proved effective in allowing flow-field-wide time-averaged discharge rate to be estimated (Harris et al. 1997a, 2000; Harris and Neri 2002; Lautze et al. 2004). Most of the satellite-derived discharge rate estimates have involved the use of 1 km pixel thermal data from AVHRR, available at least four times a day (as summarized in Table 4). During the July–August 2001 and 2002–2003 eruptions, AVHRR-derived discharge rates were calculated on a daily basis and used to update predictions for the likely maximum flow length (L). This was achieved through applying of the empirical formula proposed by Calvari and Pinkerton (1998) and corrected in Wright et al. (2001b), i.e. $L = 10^{3.11} E_r^{0.47}$. The length of 6.4 km calculated for flow fed at a peak E_r of 30 m^3/s during the 2001 eruption was in excellent agreement with its final length of 6.5 km, which meant that it stopped ~3 km short of Nicolosi.

Conclusions

A lack of precision in the measured or assumed values required to obtain reliable ground- and space-based effusion rate measurements means that estimates are usually subject to large errors and/or are quoted over a range of values. However, comparison of effusion rates measured simultaneously using ground-based techniques and/or satellite sensors show good cross-technique agreement (Table 4; Fig. 10). This agreement shows that reliable estimates can be made if each approach is applied consistently.

The three most important factors to take into account when giving an effusion rate measurement, or when using a measurement taken from the literature, are as follows.

1. The time scale of the measurement, i.e. the time-period over which a value was averaged. It then needs to be determined whether the degree of time averaging is appropriate to the application for which it is to be used.
2. The spatial scale of the measurement. Details as to whether the measurement considers total supply to the entire active flow field, or local supply to a single lava flow within that field, need to be available.
3. The measurement technique, its accompanying assumptions and potential errors.

Clarification of definitions used, as well as the temporal and spatial scales of effusion rate measurements, facilitates effusion rate measurement using well-tested formulae. Definition and technique standardization improves the quality of data for input into higher level applications that rely on volume flux data to understand and model lava flows, shallow system dynamics, as well as monitoring efforts during on-going eruptions.

Acknowledgements This paper benefited of the many discussions throughout the years with Harry Pinkerton and John Guest, and was stimulated by the many questions raised by Franco Barberi. The manuscript benefited from reviews by Dave Rothery and Lionel Wilson, as well as by Lucia Gurioli. Alessandro Bonaccorso, INGV-CT Director, is thanked for having supported and funded this research. Additional support for AJLH came from NASA Grant NNG04G064G "New Tools for Advanced Hot-Spot Tracking Using MODIS Thermal Alerts". Support for JD was provided through the Alaska Volcano Observatory and a grant from the United States Geological Survey.

References

Allard P (1997) Endogenous magma degassing and storage at Mount Etna. Geophys Res Lett 24:2219–2222

Allard P, Carbonnelle J, Metrich N, Loyer H, Zettwoog P (1994) Sulfur output and magma degassing budget of Stromboli Volcano. Nature 368:326–330

Anderson SW, Stofan ER, Plaut JJ, Crown DA (1998) Block size distributions on silicic lava flow surfaces: implications for emplacement conditions. Bull Geol Soc Am 110:1258–1267

Andres RJ, Kyle PR, Stokes JB, Rose WI (1989) SO_2 from episode 48A eruption, Hawaii: sulfur dioxide emissions from the episode 48A East Rift zone eruption of Kilauea Volcano, Hawaii. Bull Volcanol 52:113–117

Andres RJ, Rose WI, Kyle PR, deSilva S, Francis P, Gardeweg M, Moreno Roa H (1991) Excessive sulfur dioxide emissions from Chilean volcanoes. J Volcanol Geotherm Res 46:323–329

Andronico D, Branca S, Calvari S, Burton M, Caltabiano T, Corsaro RA, Del Carlo P, Garfi G, Lodato L, Miragila L, Murè F, Neri M, Pecora E, Pompilio M, Salerno G, Spampinato L (2005) A multi-disciplinary study of the 2002–03 Etna eruption: insights into a complex plumbing system. Bull Volcanol 67:314–330

Bailey JE, Harris AJL, Dehn J, Calvari S, Rowland SK (2006) The changing morphology of an open lava channel on Mt. Etna. Bull Volcanol 68:497–515

Baloga S, Pieri D (1986) Time-dependent profiles of lava flows. J Geophys Res 91:9543–9552

Baloga S, Spudis PD, Guest JE (1995) The dynamics of rapidly emplaced terrestrial lava flows and implications for planetary volcanism. J Geophys Res 100:24509–24519

Barberi F, Carapezza ML, Valenza M, Villarri L (1993) The control of lava flow during the 1991–1992 eruption of Mt. Etna. J Volcanol Geotherm Res 56:1–34

Barberi F, Brondi F, Carapezza ML, Cavarra L, Murgia C (2003) Earthen barriers to control lava flows in the 2001 eruption of Mt. Etna. J Volcanol Geotherm Res 123:231–243

Barmin A, Melnik O, Sparks RSJ (2002) Periodic behavior in lava dome eruptions. Earth Planet Sci Lett 199:173–184

Battaglia J, Aki K, Staudacher T (2005) Location of tremor sources and estimation of lava output using tremor source amplitude on the Piton de la Fournaise volcano: 2. Estimation of lava output. J Volcanol Geotherm Res 147:291–308

Behncke B, Neri M (2003) The July–August 2001 eruption of Mt. Etna (Sicily). Bull Volcanol 65:461–476

Bjornsson A, Saemundsson K, Einarsson P, Tryggvason E, Gronvold K (1977) Current rifting episode in north Iceland. Nature 266:318–322

Blake S (1990) Viscoplastic models of lava domes. In: Fink JH (ed) Lava flows and domes. Springer, Berlin Heidelberg New York, pp 88–126

Blake S, Bruno BC (2000) Modelling the emplacement of compund lava flows. Earth Planet Sci Lett 184:181–197

Booth B, Self S (1973) Rheological features of the 1971 Mount Etna lavas. Phil Trans R Soc Lond 274:99–106

Bozzo E, Coltelli M, Merlanti LSF, Tabacco I (1994) Geoelectro-magnetic survey on the lava tube of the 1991–1993 Etna eruption. Acta Vulcanol 4:125–133

Branca S, Del Carlo P (2005) Types of eruptions of Etna volcano AD 1670–2003: implications for short-term eruptive behaviour. Bull Volcanol 67:732–742

Budetta G, Del Negro C (1995) Magnetic field changes on lava flow to detect lava tubes. J Volcanol Geotherm Res 65:237–248

Burton MR, Neri M, Andronico D, Branca S, Caltabiano T, Calvari S, Corsaro RA, Del Carlo P, Lanzafame G, Lodato L, Miraglia L, Salerno G, Spampinato L (2005) Etna 2004–2005: an archetype for geodynamically-controlled effusive eruptions. Geophys Res Lett 32:L09303, DOI 10.1029/2005GL022527

Calvari S, INGV-Catania (2001) Multidisciplinary approach yields insight into Mt. Etna 2001 eruption. EOS Trans Am Geophys Un 82:653–656

Calvari S, Pinkerton H (1998) Formation of lava tubes and extensive flow field during the 1991–93 eruption of Mount Etna. J Geophys Res 103:27291–27302

Calvari S, Pinkerton H (1999) Lava tube morphology on Etna and evidence for lava flow emplacement mechanisms. J Volcanol Geotherm Res 90:263–280

Calvari S, Coltelli M, Neri M, Pompilio M, Scribano V (1994) The 1991–93 Etna eruption: chronology and geological observations. Acta Vulcanol 4:1–15

Calvari S, Neri M, Pinkerton H (2003) Effusion rate estimations during the 1999 summit eruption on Mount Etna, and growth of two distinct lava flow fields. J Volcanol Geotherm Res 119:107–123

Calvari S, Spampinato L, Lodato L, Harris AJL, Patrick MR, Dehn J, Burton MR, Andronico D (2005) Chronology and complex volcanic processes during the 2002–2003 flank eruption at Stromboli Volcano (Italy) reconstructed from direct observations and surveys with a hand-held thermal camera. J Geophys Res 110:B02201, DOI 10.1029/2004JB003129

Cashman KV, Mangan MT, Newman S (1994) Surface degassing and modifications to vesicle size distributions in active basalt flows. J Volcanol Geotherm Res 61:45–68

Chester DK, Duncan AM, Dibben C, Guest JE, Liste PH (1999) Mascali, Mount Etna region, Sicily: an example of Fascist planning during the 1928 eruption and its continuing legacy. Nat Haz 19:29–46

Costa A, Macedonio G (2005) Numerical simulation of lava flows based on depth-averaged equations. J Geophys Res 32:L05304, DOI 10.1029/2004GL021817

Crisci GM, Di Gregorio S, Rongo R, Scarpelli M, Spataro W, Calvari S (2003) Revisiting the 1669 Etnean eruptive crisis using a cellular automata model and implications for volcanic hazard in the Catania area. J Volcanol Geotherm Res 123:211–230

Crisci GM, Rongo R, Di Gregorio S, Spataro W (2004) The simulation model SCIARA: the 1991 and 2001 lava flows at Mount Etna. J Volcanol Geotherm Res 132:253–267

Crisp J, Baloga S (1990) A method for estimating eruption rates of planetary lava flows. Icarus 85:512–515

Crisp J, Baloga S (1994) Influence of crystallization and entrainment of cooler material on the emplacement of basaltic aa lava flows. J Geophys Res 99:11819–11831

Dehn J, Dean KG, Engle K, Izbekov P (2002) Thermal precursors in satellite images of the 1999 eruption of Shishaldin volcano. Bull Volcanol 64:507–519, DOI 10.1007/s00445-002-0227-0

Denlinger RP (1990) A model for dome eruptions at Mount St. Helens, Washington based on subcritical crack growth. In: Fink JH (ed) Lava flows and domes. Springer, Berlin Heidelberg New York, pp 70–87

Denlinger RP (1997) A dynamic balance between magma supply and eruption rate at Kilauea Volcano, Hawaii. J Geophys Res 102:18091–18100

Denlinger RP, Hoblitt RP (1999) Cyclic eruptive behavior of silicic volcanoes. Geology 27:459–462

Devine JD, Sigurdsson H, Davies AN, Self S (1984) Estimates of sulfur and chlorine yield to the atmosphere from volcanic eruptions and potential climatic effects. J Geophys Res 89:6309–6325

Dozier JA (1981) A method for satellite identification of surface temperature fields of subsurface resolution. Rem Sens Environ 11:221–229

Dragoni M (1989) A dynamical model of lava flows cooling by radiation. Bull Volcanol 51:88–95

Dragoni M, Tallarico A (1994) The effect of crystallization on the rheology and dynamics of lava flows. J Volcanol Geotherm Res 59:241–252

Dragoni M, Bonafede M, Boschi E (1986) Downslope flow models of a Bingham liquid: implications for lava flows. J Volcanol Geotherm Res 30:305–325

Dragoni M, Pondrelli S, Tallarico A (1992) Longitudinal deformation of a lava flow: the influence of Bingham rheology. J Volcanol Geotherm Res 52:247–254

Duncan AM, Dibben C, Chester DK, Guest JE (1996) The 1928 eruption of Mount Etna Volcano, Sicily, and the destruction of the town of Mascali. Disasters 20:1–20

Dvorak JJ, Dzurisin D (1993) Variations in magma supply rate at Kilauea Volcano, Hawaii. J Geophys Res 98:22255–22268

Dzurisin D, Koyanagi RY, English TT (1984) Magma supply and storage at Kilauea Volcano, Hawaii. J Volcanol Geotherm Res 21:177–206

Favalli M, Pareschi MT, Neri A, Isola I (2005) Forecasting lava flow paths by a stochastic approach. Geophys Res Lett 32:L03305, DOI 10.1029/2004GL021718

Fink JH (1993) The emplacement of silicic lava flows and associated hazards. In: Kilburn CRJ, Luongo G (eds) Active lavas. UCL Press, London, pp 5–24

Fink JH, Bridges NT (1995) Effects of eruption history and cooling rate on lava dome growth. Bull Volcanol 57:229–239

Fink JH, Griffiths RW (1992) A laboratory analog study of the surface morphology of lava flows extruded from point and line sources. J Volcanol Geotherm Res 54:19–32

Fink JH, Griffiths RW (1998) Morphology, eruption rates, and rheology of lava domes: insights from laboratory models. J Geophys Res 103:527–545

Fink JH, Malin MC, Anderson SW (1990) Intrusive and extrusive growth of the Mount St Helens lava dome. Nature 348:435–437

Francis P, Oppenheimer C, Stevenson D (1993) Endogenous growth of persistently active volcanoes. Nature 366:554–557

Frazzetta G, Romano R (1984) The 1983 Etna eruption: event chronology and morphological evolution of the lava flow. Bull Volcanol 47:1079–1096

Fukushima Y, Cayol V, Durand P (2005) Finding realistic models for interferometric synthetic aperture radar data: the February 2000 eruption at Piton de la Fournaise. J Geophys Res 110:B03206, DOI 10.1029/2004JB003268

Gaonac'h H, Stix J, Lovejoy S (1996) Scaling effects on vesicle shape, size and heterogeneity of lavas from Mount Etna. J Volcanol Geotherm Res 74:131–153

Glaze JA (1984) Rates of magma emplacement and volcanic output. J Volcanol Geotherm Res 20:177–211

Glaze LS, Baloga SM (2001) User's manual for lava flow path prediction algorithm. Proxemy Research, Laytonsville

Glaze LS, Anderson SW, Stofan ER, Baloga S, Smrekar SE (2005) Statistical distribution of tumuli on pahoehoe flow surfaces: analysis of examples in Hawaii and Iceland and potential applications to lava flows on Mars. J Geophys Res 110: B08202, DOI 10.1029/2004JB003564

Greeley R (1987) The role of lava tubes in Hawaiian volcanoes. US Geol Surv Prof Pap 1350:1589–1602

Greenland LP, Okamura AT, Stokes JB (1988) Constraints on the mechanics of the eruption. US Geol Surv Prof Pap 1463:155–164

Gregg TKP, Fink JH (2000) A laboratory investigation into the effects of slope on lava flow morphology. J Volcanol Geotherm Res 96:145–149

Griffiths RW, Fink JH (1992) Solidification and morphology of submarine lavas: a dependence on extrusion rate. J Geophys Res 97:19729–19737

Guest JE, Murray JB (1979) An analysis of hazard from Mount Etna volcano. Geol Soc London Mem 136:347–354

Guest JE, Wood C, Greeley R (1984) Lava tubes, terraces and megatumuli on the 1614–24 Pahoehoe lava flow field, Mount Etna, Sicily. Bull Volcanol 47:635–648

Guest JE, Kilburn CRJ, Pinkerton H, Duncan AM (1987) The evolution of lava flow-fields: observations of the 1981 and 1983 eruptions of Mount Etna, Sicily. Bull Volcanol 49:527–540

Guest JE, Spudis PD, Greeley R, Taylor GJ, Baloga SM (1995) Emplacement of xenolith nodules in the Kaupulehu lava flow, Hualalai Volcano, Hawaii. Bull Volcanol 57:179–184

Harris AJL, Neri M (2002) Volumetric observations during paroxysmal eruptions at Mount Etna: pressurized drainage of a shallow chamber or pulsed supply? J Volcanol Geotherm Res 116:79–95

Harris AJL, Rowland SK (2001) FLOWGO: a kinematic thermo-rheological model for lava flowing in a channel. Bull Volcanol 63:20–44

Harris AJL, Stevenson DS (1997) Magma budgets and steady-state activity of Vulcano and Stromboli Volcanoes. Geophys Res Lett 24:1043–1046

Harris AJL, Blake S, Rothery DA, Stevens NF (1997a) A chronology of the 1991 to 1993 Mount Etna eruption using advanced very high resolution radiometer data: implications for real-time thermal volcano monitoring. Geophys Res Lett 102:7985–8003

Harris AJL, Butterworth AL, Carlton RW, Downey I, Miller P, Navarro P, Rothery DA (1997b) Low-cost volcano surveillance from space: case studies from Etna, Krafla, Cerro Negro, Fogo, Lascar and Erebus. Bull Volcanol 59:49–64

Harris AJL, Flynn LP, Keszthelyi L, Mouginis-Mark PJ, Rowland SK, Resing JA (1998) Calculation of lava effusion rates from Landsat TM data. Bull Volcanol 60:52–71

Harris AJL, Flynn LP, Rothery DA, Oppenheimer C, Sherman SB (1999a) Mass flux measurements at active lava lakes: implications for magma recycling. J Geophys Res 104:7117–7136

Harris AJL, Wright R, Flynn LP (1999b) Remote monitoring of Mount Erebus volcano, Antarctica, using polar orbiters: progress and prospects. Int J Remote Sens 20:3051–3071

Harris AJL, Murray JB, Aries SE, Davies MA, Flynn LP, Wooster MJ, Wright R, Rothery DA (2000) Effusion rate trends at Etna and Krafla and their implications for eruptive mechanisms. J Volcanol Geotherm Res 102:237–270

Harris AJL, Flynn LP, Matías O, Rose WI (2002) The thermal stealth flows of Santiaguito: implications for the cooling and emplacement of dacitic block lava flows. Geol Soc Am Bull 114:533–546

Harris AJL, Rose WI, Flynn LP (2003) Temporal trends in lava dome extrusion at Santiaguito 1922–2000. Bull Volcanol 65:77–89

Harris AJL, Flynn LP, Matias O, Rose WI, Cornejo J (2004) The evolution of an active silicic lava flow field: an ETM+ perspective. J Volcanol Geotherm Res 135:147–168

Harris A, Bailey J, Calvari S, Dehn J (2005) Heat loss measured at a lava channel and its implications for down-channel cooling and rheology. Geol Soc Am Spec Pap 396:125–146

Harris AJL, Dehn J, Patrick MR, Calvari S, Ripepe M, Lodato L (2006) Lava effusion rates from hand-held thermal infrared imagery: an example from the June 2003 effusive activity at Stromboli. Bull Volcanol 68(2):107–117

Herd RA, Pinkerton H (1997) Bubble coalesence in basaltic lava: its impact on the evolution of bubble populations. J Volcanol Geotherm Res 75:137–157

Heslop SE, Wilson L, Pinkerton H, Head III JW (1989) Dynamics of a confined lava flow on Kilauea volcano, Hawaii. Bull Volcanol 51:415–432

Hikada M, Goto A, Umino S, Fujita E (2005) VFTS project: development of the lava flow simulation code LavaSIM with a model for three-dimensional convection, spreading, and solidification. Geochem Geophys Geosys 6:Q07008, DOI 10.1029/2004GC000896

Hon K, Kauahikaua J, Denlinger R, Mackay K (1994) Emplacement and inflation of Pahoehoe sheet flows: observations and measurements of active lava flows on Kilauea Volcano, Hawaii. Geol Soc Am Bull 106:351–370

Ishihara K, Iguchi M, Kamo K (1990) Numerical simulation of lava flows on some volcanoes in Japan. In: Fink JH (ed) Lava flows and domes. Springer, Berlin Heidelberg New York, pp 174–207

Iverson RM (1990) Lava domes modelled as brittle shells that enclose pressurized magma, with application to Mount St. Helens. In: Fink JH (ed) Lava flows and domes. Springer, Berlin Heidelberg New York, pp 47–69

Jackson DB, Swanson DA, Koyanagi RY, Wright TL (1975) The August and October 1968 east rift eruptions of Kilauea Volcano, Hawaii. US Geol Surv Prof Pap 890:1–33

Jackson DB, Hort MKG, Hon K, Kauahikaua J (1987) Detection and mapping of active lava tubes using the VLF induction technique, Kilauea Volcano, Hawaii. EOS Trans Am Geophys Union 68:1543

Jeffreys H (1925) Flow of water in an inclined channel of rectangular section. Phil Mag J Sci 49:793–807

Jurado-Chichay Z, Rowland SK (1995) Channel overflows of the Pohue Bay flow, Mauna Loa, Hawai'i: examples of the contrast between surface and interior lava. Bull Volcanol 57:117–126

Kauahikaua J, Mangan M, Heliker C, Mattox T (1996) A quantitative look at the demise of a basaltic vent: the death of Kupaianaha, Kilauea Volcano, Hawai'i. Bull Volcanol 57:641–648

Kauahikaua J, Cashman KV, Mattox TN, Heliker CC, Hon KA, Mangan MT, Thornber CR (1998) Observations of basaltic lava streams in tubes from Kilauea volcano, Island of Hawaii. J Geophys Res 103:27303–27323

Kauahikaua J, Cashman KV, Clague DA, Champion D, Hagstrum JT (2002) Emplacement of the most recent lava flows on Hualalai Volcano, Hawai'i. Bull Volcanol 64:229–253

Kauahikaua J, Sherrod DR, Cashman KV, Heliker C, Hon K, Mattox TN, Johnson JA (2003) Hawaiian lava-flow dynamics during the Pu'u 'O'o—Kupaianaha eruption: a tale of two decades. US Geol Surv Prof Pap 1676:63–87

Kazahaya K, Shinohara H, Saito G (1994) Excessive degassing of Izu-Oshima Volcano: magma convection in a conduit. Bull Volcanol 56:207–216

Kerr RC (2001) Thermal erosion by laminar lava flows. J Geophys Res 106:26453–26466

Keszthelyi L (1995) A preliminary thermal budget for lava tubes on the Earth and planets. J Geophys Res 100:20411–20420

Keszthelyi L, Self S (1998) Some physical requirements for the emplacement of long basaltic lava flows. J Geophys Res 103:27447–27464

Keszthelyi L, McEwen AS, Thordason T (2000) Terrestrial analogs and thermal models for Martian flood lavas. J Geophys Res 105:15027–15049

Kilburn CRJ (1996) Patterns and unpredictability in the emplacement of subaerial lava flows and flow fields. In: Scarpa R, Tilling RI (eds) Monitoring and mitigation of volcanic hazards. Springer, Berlin Heidelberg New York, pp 491–537

Kilburn CRJ (2000) Lava flows and flow fields. In: Sigurdsson H, Houghton B, McNutt S, Rymer H, Stix J (eds) Encyclopedia of volcanoes. Academic Press, San Diego, pp 291–305

Kilburn CRJ (2004) Fracturing as a quantitative indicator of lava flow dynamics. J Volcanol Geotherm Res 132:209–224

Kilburn CRJ, Lopes RMC (1988) The growth of aa lava fields on Mount Etna, Sicily. J Geophys Res 93:14759–14772

Kilburn CRJ, Pinkerton H, Wilson L (1995) Forecasting the behaviour of lava flows. In: McGuire B, Kilburn CRJ, Murray J (eds) Monitoring active volcanoes. UCL, London, pp 346–368

Lautze NC, Harris AJL, Bailey JE, Ripepe M, Calvari S, Dehn J, Rowland S, Evans-Jones K (2004) Pulsed lava effusion at Mount Etna during 2001. J Volcanol Geotherm Res 137:231–246

Lipman PW, Banks NG (1987) Aa flow dynamics, Mauna Loa 1984. US Geol Surv Prof Pap 1350:1527–1567

Lu Z, Masterlark T, Dzurisin D (2005) Interferometric synthetic aperture radar study of Okmok Volcano, Alaska, 1992–2003: magma supply dynamics and postemplacement lava flow deformation. J Geophys Res 1103:B02403, DOI 10.1029/2004JB003148

Macedonio G, Longo A (1999) Lava flow in a channel with a bifurcation. Phys Chem Earth 24:953–956

Madeira J, da Silveira B, Torres PC (1996) Contradicao aparente entre os volumes finais dos derrames e a estimacao das taxas de efusao: o caso da erupcao do Fogo de 1995. Simposio Internacional sobre a erupcao vulcanica de 1995 na ilha do Fogo, Cabo Verde, Lisboa, 1995:153–163

Malin MC (1980) Lengths of Hawaiian lava flows. Geology 8:306–308

Massonnet D, Briole P, Arnaud A (1995) Deflation of Mount Etna monitored by spaceborne radar interferometry. Nature 375:567–570

Matson M, Dozier J (1981) Identification of subresolution high temperature sources using a thermal IR sensor. Photogramm Eng Remote Sensing 47:1311–1318

Mattox TN, Heliker C, Kauahikaua J, Hon K (1993) Development of the 1990 Kalapana flow field, Kilauea Volcano, Hawaii. Bull Volcanol 55:407–413

Mattsson HB, Höskuldsson A (2005) Eruption reconstruction, formation of flow-lobe tumuli and eruption duration of the 5900 BP Helgafell lava field (Heimaey), South Iceland. J Volcanol Geotherm Res 147:157–172

Mayamoto H, Sasaki S (1998) Numerical simulations of flood basalt lava flows: roles of parameters on lava flow morphologies. J Geophys Res 103:27489–27502

Mazzarini F, Pareschi MT, Favalli M, Isola I, Tarquini S, Boschi E (2005) Morphology of basaltic lava channels during the Mt. Etna September 2004 eruption from airborne laser altimeter data. Geophys Res Lett 32:L04305. DOI 10.1029/2004GL021815

McClelland L, Simkin T, Summers M, Nielsen E, Stein TC (1989) Global volcanism 1975–1985. Prentice-Hall, New Jersey

Melnik O, Sparks RSJ (1999) Nonlinear dynamics of lava dome extrusion. Nature 402:37–41

Melnik O, Sparks RSJ (2005) Controls on conduit magma flow dynamics during lava dome building eruptions. Geophys Res Lett 110:B02209. DOI 10.1029/2004JB003183

Miyamoto H, Haruyama J, Kobayashi T, Suzuki K, Okada T, Nishibori T, Showman R, Lorenz AP, Mogi K, Crown DA, Rodriguez JAP, Rokugawa S, Tokunaga T, Maumoto K (2005) Mapping the structure and depth of lava tubes using ground penetrating radar. Geophys Res Lett 32:L21316. DOI 10.1029/2005GL024159

Moore HJ (1987) Preliminary estimates of the rheological properties of 1984 Mauna Loa lava. US Geol Surv Prof Pap 1350:1569–1588

Murray JB, Stevens NF (2000) New formulae for estimating lava flow volumes at Mt. Etna Volcano, Sicily. Bull Volcanol 61:515–526

Nakada S, Fujii T (1993) Preliminary report on the activity at Unzen Volcano (Japan), November 1990–November 1991: dacite lava domes and pyroclastic flows. J Volcanol Geotherm Res 54:319–333

Nakada S, Miyake Y, Sato H, Oshima O, Fujinawa A (1995) Endogenous growth of dacite dome at Unzen Volcano (Japan), 1993–1994. Geology 23:157–160

Nakada S, Shimizu H, Ohta K (1999) Overview of the 1990–1995 eruption at Unzen. J Volcanol Geotherm Res 89:1–22

Naumann T, Geist D (2000) Physical volcanology and structural development of Cerro Azul Volcano, Isabela Island, Galapagos: implications for the development of Galapagos-style shield volcanoes. Bull Volcanol 61:497–514

Nichols RL (1936) Flow-units in basalt. J Geol 44:617–630
Oddone E (1910) L'eruzione Etnea del Marzo–Aprile 1910. Boll Soc Sismol Ital 14:143–176
Ollier CD (1964) Tumuli and lava blisters of Victoria, Australia. Nature 202:1284–1286
Oppenheimer C (1991) Lava flow cooling estimated from Landsat Thematic Mapper infrared data: the Lonquimay eruption (Chile, 1989). J Geophys Res 96:21865–21878
Oppenheimer C, Francis PW, Rothery DA, Carlton RWT, Glaze LS (1993) Infrared image analysis of volcanic thermal features: Lascar Volcano, Chile, 1984–1992. J Geophys Res 98:4269–4286
Patrick MR, Dehn J, Papp KR, Lu Z, Dean K, Moxey L, Izbekov P, Guritz R (2003) The 1997 eruption of Okmok Volcano, Alaska: a synthesis of remotely sensed imagery. J Volcanol Geotherm Res 127:87–105
Peterson DW, Holcomb RT, Tilling RI, Christiansen RL (1994) Development of lava tubes in the light of observations at Mauna Ulu, Kilauea Volcano, Hawaii. Bull Volcanol 56:343–360
Pieri DC, Baloga SM (1986) Eruption rate, area, and length relationships for some Hawaiian lava flows. J Volcanol Geotherm Res 30:29–45
Pinkerton H (1993) Measuring the properties of flowing lavas. In: Kilburn CRJ, Luongo G (eds) Active lavas. UCL Press, London, pp 175–191
Pinkerton H, Sparks RSJ (1976) The 1975 subterminal lavas, Mount Etna: a case history of the formation of a compound lava field. J Volcanol Geotherm Res 1:167–182
Pinkerton H, Wilson L (1994) Factors affecting the lengths of channel-fed lava flows. Bull Volcanol 56:108–120
Richter DH, Eaton JP, Murata KJ, Ault WU, Krivoy HL (1970) Chronological narrative of the 1959–60 eruption of Kilauea Volcano, Hawaii. US Geol Surv Prof Pap 537:1–73
Ripepe M, Marchetti M, Ulivieri G, Harris A, Dehn J, Burton M, Caltabiano T, Salerno G (2005) Effusive to explosive transition during the 2003 eruption of Stromboli volcano. Geology 33:341–344
Romano R, Sturiale C (1982) The historical eruptions of Mt. Etna. Mem Soc Geol Ital 23:75–97
Rose WI (1972) Pattern and mechanism of volcanic activity at the Santiaguito volcanic dome, Guatemala. Bull Volcanol 36:73–94
Rossi MJ (1997) Morphology of the 1984 open-channel lava flow at Krafla Volcano, Northern Iceland. Geomorphol 20:95–112
Rossi MJ, Gudmundsson A (1996) The morphology and formation of flow-lobe tumuli on Icelandic shield volcanoes. J Volcanol Geotherm Res 72:291–308
Rothery DA, Francis PW, Wood CA (1988) Volcano monitoring using short wavelength infrared data from satellites. J Geophys Res 93:7992–8008
Rowland SK (1996) Slopes, lava flow volumes, and vent distributions on Volcan Fernandina, Galapagos Islands. J Geophys Res 101:27657–27672
Rowland SK, Munro DC (1993) The 1919–1920 eruption of Mauna Iki, Kilauea: chronology, geologic mapping, and magma transport mechanisms. Bull Volcanol 55:190–203
Rowland SK, Walker GPL (1990) Pahoehoe and aa in Hawaii: volumetric flow rate controls the lava structure. Bull Volcanol 52:615–628
Rowland SK, MacKay ME, Garbeil H, Mouginis-Mark PJ (1999) Topographic analyses of Kilauea Volcano, Hawai'i, from interferometric airborne radar. Bull Volcanol 61:1–14
Rowland SK, Harris AJL, Wooster MJ, Amelung F, Garbeil H, Wilson L, Mouginis-Mark PJ (2003) Volumetric characteristics of lava flows from interferometric radar and multispectral satellite data. Bull Volcanol 65:311–330
Rowland SK, Harris AJL, Garbeil H (2004) Effects of Martian conditions on numerically modeled, cooling-limited, channelized lava flows. J Geophys Res 109:E10010. DOI 10.1029/2004JE002288
Rowland SK, Garbiel H, Harris AJL (2005) Lengths and hazards from channel-fed lava flows on Mauna Loa, Hawai'i, determined from thermal and downslope modeling with FLOWGO. Bull Volcanol 67:634–647
Sakimoto SEH, Zuber MT (1998) Flow and convective cooling in lava tubes. J Geophys Res103:27465–27487
Schwarz C (1993) The Chambers dictionary. Chambers Harrap, Edinburgh
Self S, Thordarson T, Keszthelyi L, Walker GPL, Hon K, Murphy MT, Long P, Finnemore S (1996) A new model for the emplacement of Columbia River Basalt as large, inflated Pahoehoe lava flow fields. J Geophys Res 23:2689–2692
Self S, Thordarson T, Keszthelyi L (1997) Emplacement of continental flood basalt lava flows. Am Geophys Union Monograph 100:381–410
Smith SJ (2005) Chronologic multisensor assessment for Mount Cleveland, Alaska from 2000 to 2004 focusing on the 2001 eruption. MS thesis, University of Alaska, Fairbanks
Soule SA, Cashman KV, Kauahikaua JP (2004) Examining flow emplacement through the surface morphology of three rapidly emplaced, solidified lava flows, Kilauea Volcano, Hawai'i. Bull Volcanol 66:1–14
Soule SA, Fornari DJ, Perfit MR, Tivey MA, Ridley WI, Schouten H (2005) Channelized lava flows at the East Pacific Rise crest 9°–10°N: the importance of off-axis lava transport in developing the architecture of young oceanic crust. Geochem Geophys Geosys 6:Q08005. DOI 10.1029/2005GC00912
Sparks RSJ, Young SR, Barclay J, Calder ES, Cole P, Darroux B, Davies MA, Druitt TH, Harford C, Herd R, James M, Lejeune AM, Loughlin S, Norton G, Skerrit G, Stasiuk MV, Stevens NS, Toothill J, Wadge G, Watts R (1998) Magma production and growth of the lava dome of the Soufriere Hills Volcano, Monsterrat, West Indies: November 1995 to December 1997. Geophys Res Lett 25:3421–3424
Stasiuk MV, Jaupart C (1997) Lava flow shapes and dimensions as reflections of magma system conditions. J Volcanol Geotherm Res 78:31–50
Steffke AM (2005) Temperatures, thermal fluxes and effusion rates associated with the growth of Bezymianny volcano using spaceborne thermal infrared data. MS Thesis, University of Alaska, Fairbanks
Stevens NF, Murray JB, Wadge G (1997) The volume and shape of the 1991–1993 lava flow field at Mount Etna, Sicily. Bull Volcanol 58:449–454
Stevens NF, Wadge G, Murray JB (1999) Lava flow volume and morphology from digitised contour maps: a case study from Mount Etna, Sicily. Geomorphol 28:251–261
Stoiber RE, Williams SN, Huebert BJ (1986) Sulfur and halogen gases at Masaya caldera complex, Nicaragua: total flux and variations with time. J Geophys Res 91:12215–12231
Sutton AJ, Elias T, Gerlach TM, Stokes JB (2001) Implications for eruptive processes as indicated by sulfur dioxide emissions from Kilauea Volcano, Hawai'i, 1979–1997. J Volcanol Geotherm Res 108:283–302
Sutton AJ, Elias T, Kauahikaua J (2003) Lava-effusion rates for the Pu'u 'O'o–Kupaianaha eruption derived from SO_2 emissions and very low frequency (VLF) measurements. US Geol Surv Prof Pap 1676:137–148
Swanson DA, Holcomb RT (1990) Regularities in growth of the Mount St. Helens dacite dome, 1980–1986. In: Fink JH (ed) Lava flows and domes. Springer, Berlin Heidelberg New York, pp 3–24
Swanson DA, Duffield WA, Jackson DB, Peterson DW (1979) Chronological narrative of the 1969–71 Mauna Ulu eruption of Kilauea volcano, Hawaii. US Geol Surv Prof Pap 1056:1–55

Tallarico A, Dragoni M (1999) Viscous Newtonian laminar flow in a rectangular channel: application to Etna lava flows. Bull Volcanol 61:40–47

Tanguy JC, Kieffer G, Pantanè G (1996) Dynamics, lava volume and effusion rate during the 1991–1993 eruption of Mount Etna. J Volcanol Geotherm Res 71:259–265

Thordason T, Self S (1996) Sulfur, chlorine and fluorine degassing and atmospheric loading by the Roza eruption, Columbia River Basalt Group, Washington, USA. J Volcanol Geotherm Res 74:49–73

Thordason T, Self S (1998) The Roza member, Columbia River Basalt Group: a gigantic Pahoehoe lava flow field formed by endogenous processes? J Geophys Res 103:21411–27445

Tilling RI (1987) Fluctuations in surface height of active lava lakes during the 1972–1974 Mauna Ulu eruption, Kilauea Volcano, Hawaii. J Geophys Res 92:13721–13730

Tilling RI, Peterson DW (1993) Field observations of active lava in Hawaii: some practical considerations. In: Kilburn CRJ, Luongo G (eds) Active lavas. UCL Press, London, pp 147–174

Tilling RI, Christansen RL, Duffield WA, Endo ET, Holcomb RT, Koyanagi RY, Peterson DW, Unger JD (1987) The 1972–1974 Mauna Ulu eruption, Kilauea Volcano: an example of quasi-steady-state magma transfer. US Geol Surv Prof Pap 1350:405–469

Tryggvason E (1986) Multiple magma reservoirs in a rift zone volcano: ground deformation and magma transport during the September 1984 eruption of Krafla, Iceland. J Volcanol Geotherm Res 28:1–44

Wadge G (1977) The storage and release of magma on Mount Etna. J Volcanol Geotherm Res 2:361–384

Wadge G (1978) Effusion rate and the shape of aa lava flow-fields on Mount Etna. Geology 6:503–506

Wadge G (1981) The variation of magma discharge during basaltic eruptions. J Volcanol Geotherm Res 11:139–168

Wadge G (1982) Steady state volcanism: evidence from eruption histories of polygenetic volcanoes. J Geophys Res 87:4035–4049

Wadge G (1983) The magma budget of Volcan Arenal, Costa Rica from 1968 to 1980. J Volcanol Geotherm Res 19:281–302

Wadge G, Walker GPL, Guest JE (1975) The output of the Etna volcano. Nature 255:385–387

Wadge G, Young PAV, McKendrick IJ (1994) Mapping lava flow hazards using computer simulation. J Geophys Res 99:489–504

Walker GPL (1973) Lengths of lava flows. Phil Trans R Soc Lond 274:107–118

Walker GPL (1991) Structure, and origin by injection of lava under surface crust, of tumuli, "lava rises," "lava-rise pits," and "lava-inflation clefts" in Hawaii. Bull Volcanol 53:546–558

Wilmoth RA, Walker GPL (1993) P-type and S-type pahoehoe: a study of vesicle distribution patterns in Hawaiian lava flows. J Volcanol Geotherm Res 55:129–142

Wolfe EW, Neal CA, Banks NG, Duggan TJ (1988) Geological observations and chronology of eruptive events. US Geol Surv Prof Pap 1463:1–97

Woodcock D, Harris AJL (2005) The dynamics of a channel-fed lava flow on Pico Partido Volcano, Lanzarote: evidence for a hydraulic jump? Bull Volcanol 69:207–215

Wright R, Blake S, Harris AJL, Rothery DA (2001a) A simple explanation for the space-based calculation of lava eruption rates. Earth Planet Sci Lett 192:223–233

Wright R, Flynn LP, Harris AJL (2001b) The evolution of lava flow-fields at Mount Etna, 27–28 October 1999, observed by Landsat 7 ETM+. Bull Volcanol 63:1–7

Young P, Wadge G (1990) FLOWFRONT: simulation of a lava flow. Comp Geosci 16:1171–1191

Zebker HA, Rosen P, Hensely S, Mouginis-Mark PJ (1996) Analysis of active lava flows on Kilauea Volcano, Hawaii, using SIR-C radar correlation measurements. Geology 24:495–498